ORIGINAL ARTICLE

How climate change is affecting the summer monsoon extreme rainfall pattern over the Indo-Gangetic Plains of India: present and future perspectives

Manas Pant[1,2] · R. Bhatla[1,2] · Soumik Ghosh[3] · Sushant Das[4,5] · R. K. Mall[2]

Abstract

The Indo-Gangetic Plain (IGP), the source of grains for around 40% Indian population, is known as the breadbasket of India. The Indian Summer Monsoon Rainfall (ISMR) plays a vital role in the agricultural activities in this region. The rapid urbanization, land use and land cover change have significantly impacted the region's agriculture, water resources, and socio-economic facets. The present study has investigated the observed and regional modeling aspects of ISMR characteristics, associated extremes over the IGP, and future perspectives under the high-emission RCP8.5-scenario. Future projections suggest a 10–20% massive decrease during pre-monsoon (March–May) and earlier ISM season months (i.e., June and July). A significant 40–70% decline in mean monsoon rainfall during the June–July months in the near future (NF; 2041–2060) has been projected compared to the historical period (1986–2005). An abrupt increase of 80–170% in mean monsoon rainfall during the post-monsoon (October–December) in the far future (FF; 2080–2099) is also projected. The distribution of projected extreme rainfall events shows a decline in moderate or rather heavy events (5 or more) in NF and FF. Further, an increase in higher rainfall category events such as very heavy (5–10) and extremely heavy rainfall (5 or more) events in NF and FF under the warmer climate is found. However, the changes are less prominent during FF compared to the NF. The mean thresholds for extremely heavy rainfall may increase by 1.9–4.9% during NF and FF. Further, the evolution patterns of various quantities, such as tropospheric temperature gradient (TG), specific humidity, and mean sea level pressure, have been analyzed to understand the physical processes associated with rainfall extremes. The strengthening in TG and enhanced atmospheric moisture content in NF and FF support the intensification in projected rainfall extremes over IGP.

Keywords Monsoon extreme · Indian summer monsoon rainfall (ISMR) · Indo-Gangetic Plain (IGP) · REGional Climate Model v 4.7 (RegCM4.7) · RCP8.5 scenario · CORDEX-CORE

✉ Soumik Ghosh
soumik.ghosh@fulbrightmail.org;
soumik.ghosh@weizmann.ac.il

1 Department of Geophysics, Banaras Hindu University, Varanasi, India

2 DST-Mahamana Centre of Excellence in Climate Change Research, Institute of Environment and Sustainable Development, Banaras Hindu University, Varanasi, India

3 Department of Earth and Planetary Sciences, Weizmann Institute of Science, Rehovot, Israel

4 Earth System Physics Section, The Abdus Salam International Centre for Theoretical Physics, Trieste, Italy

5 Present Address: Department of Earth and Atmospheric Sciences, National Institute of Technology, Rourkela, Odisha, India

1 Introduction

The Indian summer monsoon (ISM) season consists of different epochs, including evolution, advancement, and withdrawal (Rajeevan et al. 2010; Bhatla et al. 2016), determining rainfall amount and duration across India. Moreover, the rainfall during the ISM season undergoes temporal and spatial variations, making the ISM system complex, engaging, and essential (Gadgil 2003). Several modeling approaches are considered to understand the monsoon dynamics and impact of climate change using the global (e.g., Parth Sarthi et al. 2015, 2016) and regional climate model (Sinha et al. 2013; Bhatla et al. 2016; Ghosh et al. 2019, 2022, 2023; Dash et al. 2015; Verma and Bhatla 2021; Shahi et al. 2021). They conclude that the dynamics of the ISM circulation are greatly influenced by various factors spanning from global

scales, such as El-Nino Southern Oscillations (ENSO), to regional scales, including topography, land use, urbanization, and aerosols. The rise of greenhouse gas (GHG) levels disrupts atmospheric thermodynamic and dynamic processes, leading to abnormal alterations in regional and global monsoon systems (Field et al. 2012). The Indo-Gangetic Plain (IGP) region of India could be the best example to see this impact as this region is of great relevance to South Asia's food security as it contributes a significant share of the national GDP of the country India and is popularly known as the "Food Basket of India" (Koshal 2014). Any discrepancy in the rainfall pattern may negatively affect agriculture, the economy, and the population of the region.

The access to the ISM circulations and patterns along with associated inter-annual and intra-seasonal variations using regional climate model (RegCM) over the Coordinated Regional Climate Downscaling Experiment (CORDEX; 22 °S–50°N; 10°E–130°E) region has been considered by many researchers (Dash et al. 2015; Bhatla et al. 2016, 2018, 2019; Das et al. 2020; Rai et al. 2020; Ghosh et al. 2019, 2022, 2023). They suggest an improvement in the model's performance in simulating the rainfall characteristics by using the concept of mixing of the parameterization over the subcontinent (Giorgi et al. 2012), and successfully set up the experiment to understand the seasonal and intraseasonal monsoon characteristics over India (Bhatla et al. 2016; Ghosh et al. 2019, 2022, 2023; Sinha et al. 2019; Mishra et al. 2020; Shahi et al. 2021; Verma and Bhatla 2021; Verma et al. 2021) and over the monsoon core region (MCR) (Ghosh et al. 2019). Ngo-Duc et al. (2017) and Pant et al. (2022, 2023) have employed the same regional model over Southeast Asia CORDEX domain and found that RegCM can reproduce climate extremes over a complex topography. Recently, Shahi et al. (2021) have proposed that RegCM can simulate the projected rise in extreme rainfall events over India and MCR in the future under intense warming scenarios (refer to Figs. 5 and 12). Using the updated version of the RegCM, Pant et al. (2022) have found the model's suitability in capturing the extreme event over the Indian subcontinent, which further motivates to focus on capturing the localized extreme rainfall events during the monsoon season (Pant et al. 2023). They successfully implemented the mixed parameterization concept in RegCM4.7 to capture the localized extreme rainfall events over the region, like IGP. However, these studies highlight the suitability of regional evaluation, but socio-economically important part like IGP has received less attention to date.

In the last few years, the country has faced several devastating rainfall events, affecting millions of lives. Several studies have shown a linkage between the increase in the number of extreme events and global climate warming, as the warming leads to the enhancement of moisture content in the atmosphere (Goswami et al. 2006; Rajeevan et al. 2008;

Ajayamohan and Rao 2008; Ghosh et al. 2012; Tabari 2020). The long-term studies of global surface soil moisture, precipitation, evapotranspiration, and vegetation index have shown that about 48% of vegetated areas experienced drying. In comparison to it, 9% showed wetting patterns in the past 40 years. Decreasing precipitation and increasing evapotranspiration associated with drying soil indicate potential challenges for future global soil water management (Piao et al. 2009; Lal et al. 2023). The moisture flux convergence is found to be more influential for heavier rainfall probabilities, in contrast, soil moisture has a weaker effect on rainfall probability, particularly for intermediate-to-heavy rainfall events (Wei et al. 2016).

In recent decades, enhanced irregularity and variability in ISM rainfall (ISMR) have amplified the frequency and intensity of extreme events like floods and droughts (Annamalai and Sperber 2005; Lau and Waliser 2011). Roxy et al. (2017) have found evidence of a gradual decline of about 10–20% in ISMR and a three-times increase in extreme rainfall over the MCR. By using the India Meteorological Department (IMD)'s criteria for rain (see Sect. 2), Pattanaik and Rajeevan (2010) have found a significant decreasing trend in moderately heavy rainfall events. In contrast, extremely heavy rainfall events have shown an increasing trend in India. The 2005 Mumbai floods (Kumar et al. 2008; Pant et al. 2022), the 2013 Uttarakhand disaster (Joseph et al. 2015), the India-Pakistan floods in 2014, the 2015 Chennai flood (Boyaj et al. 2018), and the Kerala floods in 2018 (Mishra and Shah 2018) are some of the examples of most annihilating extreme rainfall events in the history of the country. The decrease in mean ISMR and increase in heavy rainfall episodes can be attributed to Indian Ocean warming, land use change, convective available potential energy increase, low-level moisture convergence, more frequent ENSO events, and increased atmospheric aerosols (Kulkarni 2012; Kumar et al. 2006; Roxy et al. 2014, 2015; Singh et al. 2014). In addition, Nikumbh et al. (2019) have suggested a low-pressure monsoon system to significantly increase occurrences of widespread heavy rainfall episodes across the country. Therefore, more attention toward climate projections of changes in rainfall patterns and associated extreme under-warming scenarios is necessary (Field et al. 2012; Collins et al. 2013).

The ISMR variability and associated features over the IGP regions are well documented by Kothyari et al. (1997); Sinha and Jain (1998); Adel (2002); Singh and Sontakke (2002). A significant shift towards western regions in rainfall and heavy rainfall activities has also been found over the IGP (Singh and Sontakke 2002). Bhatla et al. (2019) have studied the long-term trends in different category rainfall events over IGP and have found moderate rainfall events (36.5–64.4 mm or less) show increasing trends, whereas heavy (64.5–124.4 mm) to very heavy (124.5–244.4 mm)

rainfall events reported decreasing over the IGP during the period 1901–2010. Pant et al. (2023) have presented a detailed rainfall assessment by using various climate indices and found projected enhancement in 90th and 99th percentile rainfall days, whereas a decline in the number of wet days and mean ISMR with RegCM4.7 in the future under high-emission RCP8.5 scenario. However, changes in the frequency and intensity of extreme rainfall events, changes in seasonal extreme rainfall patterns, and governing physical processes over IGP in a warming climate remain largely unrecognized. The model capacity in recognizing the IMD's categorical extremes is another remaining part yet to be investigated over the important region like IGP. Furthermore, how climate change affects the summer monsoon extreme rainfall pattern over the IGP needs critical attention. Considering these factors, an attempt is made to investigate the monsoon rainfall in point of the historical and future aspects and associated extremes under the high-emission scenario (RCP8.5). In that view, the authors have investigate the past and future perspective of seasonal rainfall patterns and extreme rainfall events using RegCM4.7 over the IGP region, which is 13% of the total geographical area of the country and extends up to the northern, central, and eastern regions and presents the place of importance by itself for India.

2 Model description, data, and methodology

2.1 Model description

The present study utilizes the 4.7 version of the Regional Climate Model (i.e., RegCM4.7) developed at Abdus Salam International Centre for Theoretical Physics (ICTP). Being a limited area sigma-coordinate model, RegCM4.7 has been extensively downscaled over the south Asia CORDEX domains to access the climatic information at the regional scale (Giorgi et al. 2012). For the representation of the land surface processes, RegCM4.7 has been coupled with the Community Land Model version 4.5 (CLM4.5; Oleson et al. 2013). Subgrid Explicit Moisture Scheme (SUBEX) is considered a large-scale precipitation scheme (Pal et al. 2000), whereas the Planetary Boundary Layer (PBL) scheme is given by Grenier and Bretherton (2001). Additional model configuration details have been listed in Table 1 and described by Elguindi et al. (2013).

Sharmila et al. (2015) found that the simulations of MPI_ESM-MR, MIROC5, and NOR-ESM1-M GCMs provide a more accurate depiction of the circulation features of the ISMR characteristics. Therefore, only those simulations denoted as RegCM_EIN75, RegCM_MPI, RegCM_MIROC, and RegCM_NOR are considered for this study. For this purpose, the initial and boundary conditions (ICBCs) forced using the 6-hourly ICBCs obtained from the European Center for Medium-Range Weather Forecast (ECMWF) ERA-Interim ($\sim 0.75° \times 0.75°$) (hereafter EIN75), Max Planck Institute for Meteorology Earth System Model MR (MPI-ESM-MR; Watanabe and Opper 2010) with resolution $\sim 1.8° \times 1.8°$, Model for Interdisciplinary Research on Climate 5 (MIROC5; Stevens et al. 2013) with resolution $\sim$ T85L40 for atmosphere and $\sim 1° \times 1°$ for the ocean, and the Norwegian Earth System Model (NOR-ESM1-M; Bentsen et al. 2013) with resolution $\sim 2° \times 2°$ for atmosphere and $\sim 1° \times 1°$ for ocean. A previous study by Ghosh et al. (2019) shows the importance of the mix parameterization scheme, and the precaution from the ICBC is considered for a reliable ISM simulation. Based on their suggestion of a mixed parameterization scheme, considering the Emanuel parameterization (Emanuel and Živković-Rothman 1999) over land and Tiedtke (Tiedtke 1989) over the ocean has employed for the cumulus convection. The model is dynamically downscaled at 25 km horizontal resolution and 23 vertical levels under CORDEX-CORE protocols. The model is set up with free run using the EIN75 ICBCs from 1979, where the first 7 years of simulation is considered the spin-up period for this study. Further, for the GCM downscaling, the data sets

Table 1 Detailed RegCM4.7 model description

Model dynamics	Hydrostatic
Horizontal and vertical resolution	25 km with 23 vertical sigma levels
Initial and lateral boundary conditions	(1) EIN75, (2) MPI-ESM-MR, (3) MIROC5, and (4) NorESM1-M
Sea surface temperature	EIN75
Radiation scheme	NCAR Community Climate Model 3 (CCM3; Kiehl et al. 1996)
Land surface model	Community land model version 4.5 (CLM4.5; Oleson et al. 2013)
Planetary boundary layer scheme (PBL)	Grenier and Bretherton (2001)
Large –Scale Precipitation Scheme	Subgrid Explicit Moisture Scheme (SUBEX) (Pal et al. 2000)
Convective parametrization scheme	MIT Emanuel (Emanuel and Živković-Rothman 1999) over land; Tiedtke (1989) over ocean

are available from 1970, thus first 16 years have been considered as the model spin-up time.

2.2 Data and methodology

The high-resolution (0.25° × 0.25°) gridded daily rainfall data set provided by the IMD (Pai et al. 2014) is considered for the reference period of 1986–2005 and the model validation. The three-time slices are chosen with 20 years each, i.e., 1986–2005 for the historical and reference period, 2041–2060 for the near future (NF), and 2080–2099 for the far future (FF) under RCP8.5 high emission scenario. The model domain, topography (South-Asia CORDEX domain), and the study region (i.e., IGP) have been shown in Fig. 1.

The model simulated annual cycle of rainfall is analyzed with the monthly variation of rainfall over the IGP region. The different category rainfall events, classified using the IMD rainfall criteria, are counted by providing different threshold values for each time period. Further, to understand the occurrence of rainfall extremes and changes in NF and FF over IGP, the composite patterns of tropospheric temperature gradient (TG; between 700 hPa and 925 hPa), specific humidity (hus; at 850 hPa), mean sea level pressure (MSLP), and the wind (u &v, at 850 hPa) during extreme rainfall days have been computed.

2.2.1 Classification of rainfall events

The identification and characterization of extreme rainfall events are considered using the IMD's criteria, where different category events based on rainfall reported in a day have been defined (Source: http://imd.gov.in/section/nhac/

termglossary.pdf). The rainfall amount of 35.6–64.4 mm, 64.5–124.4 mm, 124.5–244.4 mm, and 244.5 mm or more in a day are termed as rather heavy rainfall (RHR), heavy rainfall (HR), very heavy rainfall (VHR) and extremely heavy rainfall (EHR) events respectively (Barde et al. 2020) (Table 2).

2.2.2 Diagnostic and model validation tools

Various statistical techniques are considered to evaluate the model performance, namely the correlation coefficient (CC), root mean square error (RMSE), and standard deviation (SD). Further, the modified index of agreement (MD) is considered to check the model skill. The probability density function (PDF) represents the distribution of extreme rainfall events over the study region. The relative changes in % are calculated to assess the rainfall amount changes in the projected future. Further, the two-tailed Student's t-test hypothesis is considered to understand the significance level of the model data (Fadem 2012).

Modified index of agreement (MD) The MD is one of the most useful statistical techniques to measure model skills

Table 2 The IMD's criteria for different category rainfall events (based on the total rainfall reported (mm) in a day

Descriptive term used	Rainfall amount in mm
Rather heavy rainfall event	35.6–64.4
Heavy rainfall event	64.5–124.4
Very heavy rainfall event	124.5–244.4
Extremely heavy rainfall event	> 244.5
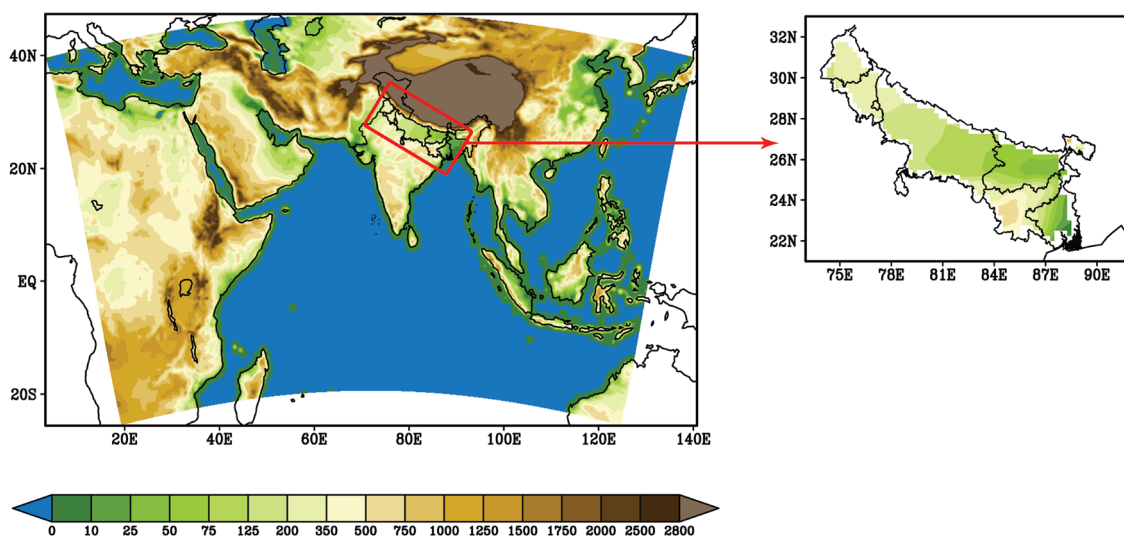
Fig. 1 Topography of South-Asia CORDEX domain (22° S–50° N; 10° E–130° E) considered as a model domain. The small rectangular box shows the study region (IGP) highlighted on the right side of the figure

(Willmott 1981). The values for MD vary from 0 (no agreement) to 1 (best agreement) and are given as,

$$MD = 1 - \frac{\sum_{i=1}^{N} |Obs_i - Mod_i|}{\sum_{i=1}^{N} |Mod_i - \overline{Mod}| + |Obs_i - \overline{Obs}|}$$

where *Obs* stands for observations, *Mod* stands for model simulations, while $\overline{Obs}$ and $\overline{Mod}$ are their average values, respectively.

Probability density distribution function The normal distribution is the most useful continuous distribution among all the distributions (Amin et al. 2016). The PDF of the normal distribution is given as,

$$f(x) = \frac{e^{-\frac{1}{2}(\frac{x-\mu}{\sigma})^2}}{\sigma\sqrt{2\pi}}$$

where μ and σ are the mean and standard deviation of the population, respectively.

Relative changes The relative changes (in %) are calculated to assess the variations/changes in rainfall amount during the projected future time slices compared to the historical period.

$$Relative\ change\ (\%) = \frac{Future - Historical}{Historical} \times 100$$

3 Results and analysis

3.1 Model evaluation

The annual cycle of rainfall averaged over IGP during the historical period (1986–2005) is illustrated in Fig. 2. IMD Observation reports an increase in rainfall for June. It reaches its maximum (9 mm/day) during July and decreases after September. The figure shows that the IGP region
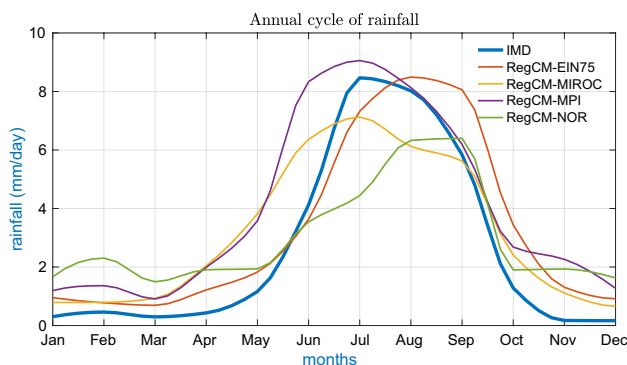

Fig. 2 The annual cycle of observed as well as RegCM4.7 simulated rainfall climatology (mm/day) for four different GCM forcing over the IGP during the historical period of 1986–2005

receives maximum rainfall during June, July, August, and September (JJAS), i.e., the ISM season. However, rainfall amounts are greater in later monsoon months compared to the earlier months, which can be explained by several studies, and the authors have proposed a delay in monsoon onset with a decline in ISMR (Ashfaq et al. 2021; Reshma et al. 2021). All the considered RegCM4.7 experiments have reproduced a similar pattern of rainfall satisfactorily. However, slight overestimation/underestimation (1–2 mm/day) in rainfall amount exists during JJAS among all the RegCM simulations compared to the observations. The downscaled RegCM_EIN75 and RegCM_MPI show a more realistic pattern. In contrast, the other two downscales, namely RegCM_MIROC and RegCM_NOR, have shown an underestimation (maximum rainfall ∼7 mm/day) in simulating the maximum rainfall during monsoon season. Further, each model's performance is similar and in accordance with the observation during the winter and post-monsoon seasons. The overall analysis suggests that among all the considered RegCM4.7 simulations, RegCM_EIN75 and RegCM_MPI have shown the best skills in simulating the annual cycle of rainfall over IGP during the historical period.

The validation of RegCM4.7 downscaling with different forcing combinations has been illustrated in Fig. 3i–iii. The spatial pattern of CC, RMSE, and SD of different model simulations with IMD data during the historical period (1986–2005) over IGP has been depicted in Fig. 3i. The MD is printed in the panel. The RegCM_EIN75 has shown 0.9 or more CC over most regions, especially lower and central IGP (Fig. 3ia). However, a lesser CC (< 0.6) can be noticed over the upper IGP region. The RMSE, SD, and MD values for RegCM_EIN75 are 1.78, 2.97, and 0.79, respectively. The RegCM_MPI shows CC values ranging from 0.7 to 0.9 over most central and lower IGP regions (Fig. 3ib). In contrast, it shows significantly less CC <0.6 over upper IGP regions along with RMSE, SD, and MD values of 2.19, 3.60, and 0.71, respectively. The member RegCM_MIROC shows CC ranging from 0.5 to 0.8 over most of the central and lower IGP regions, while the upper parts depicted very less CC (< 0.5) (Fig. 3ic). The RMSE and SD values are 1.78 and 2.97, respectively, while MD ∼0.75 is found for the RegCM_MIROC model. Similarly, RegCM_NOR shows the CC range between 0.5 and 0.8 over some regions of central IGP, whereas it shows significantly less CC over the upper and lower IGP regions (Fig. 3id). The RegCM_NOR shows RMSE, SD, and MD values of 1.95, 2.35, and 0.66, respectively. The discussion suggests a satisfactory performance using the RegCM4.7 downscaling experiment with each downscaling regarding CC, RMSE, and SD (3.24 for IMD). However, RegCM_EIN75 and RegCM_MPI have shown more efficiency in reproducing the rainfall over the IGP.

The JJAS mean rainfall and mean bias is considered for different RegCM simulations over IGP during the historical

Model Validation

(i) Correlation

(ii) Mean(mm/day)

(iii) Mean Bias(mm/day)
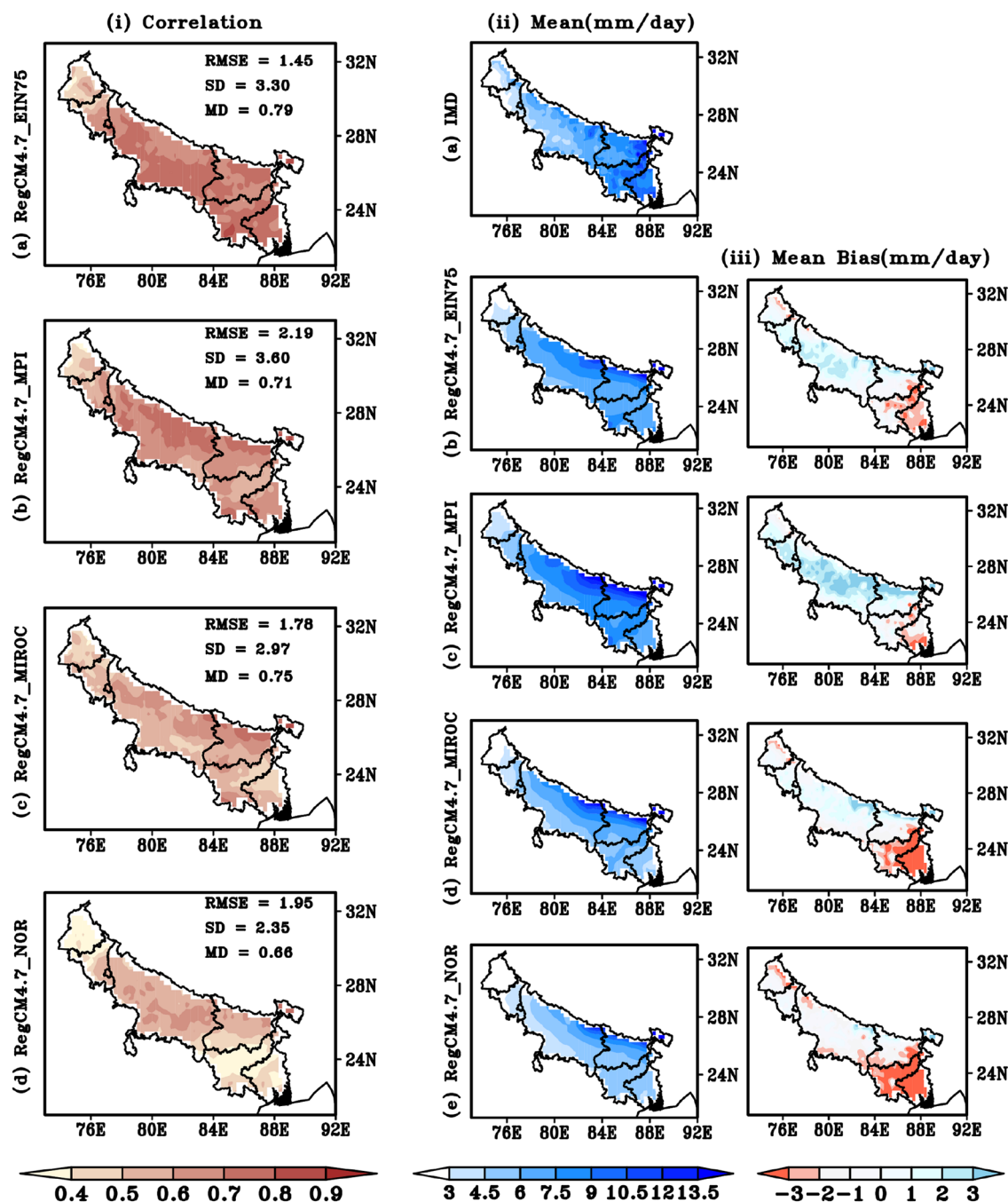
Fig. 3 i The spatial distribution of correlation coefficient (CC) between IMD rainfall and RegCM4.7 simulated rainfall using four different forcings viz. **a** RegCM_EIN75, **b** RegCM_MPI, **c** RegCM_MIROC and **d** RegCM_NOR during the historical period (1986–2005). The printed values in each panel depict the RMSE, SD, and MD of respective downscaling experiments with the observed (IMD) rainfall. **ii** Seasonal mean monsoon rainfall pattern (mm/day) of **a** observations (IMD), **b** RegCM_EIN75, **c** RegCM_MPI, **d** RegCM_MIROC, and **e** RegCM_NOR. **iii** Mean rainfall bias from observed rainfall over the IGP during the historical period (1986–2005) for the respective model simulation

period of 1986–2005 (Fig. 3ii, iii). The IMD observation shows rainfall in the 3–14 mm/day or more range, which is satisfactorily simulated by all the RegCM4.7 experiments (Fig. 3ii). Most lower and central IGP regions have received rainfall in the 5–13.5 mm/day or more, whereas upper IGP regions reported fewer rainfall amounts ranging from 2–5 mm/day. The RegCM_EIN75 has satisfactorily simulated the rainfall pattern of the entire IGP along with some overestimation over central IGP (Fig. 3ii(b)). As far as the mean bias is concerned, RegCM_EIN75 shows dry bias (− 1 to − 3 mm/day) over some lower IGP regions, whereas more negligible wet bias ranging from 1–3 mm/day over a few central and upper IGP regions (Fig. 3iii(b)). The member RegCM_MPI reported 6–11 mm/day rainfall over lower and central IGP regions, whereas 3–6 mm/day over the upper IGP regions (Fig. 3ii(c)). A smaller amount of wet bias (− 1 to − 3 mm/day) can be noticed over some lower areas of IGP. At the same time, most of the IGP (including central and upper regions) reported moderately wet to wetter bias in the range of 1–3 mm/day (Fig. 3iii(c)). Similarly, the member RegCM_MIROC simulates the rainfall in the range of 6–11 mm/day over northern regions of central and lower IGP while 2–5 mm/day over upper IGP and some southern central and lower IGP regions (Fig. 3ii(d)). Similar to the other experiments, RegCM_MIROC also shows dry bias (− 1 to − 3 mm/day) over most of the lower IGP

regions, while a significant wet tendency (~1–3 mm/day) can be noticed over a few northern lower and central IGP regions (Fig. 3iii(d)). The member RegCM_NOR underestimates the rainfall over lower IGP except for a few north regions. The RegCM_NOR has reproduced rainfall ranging from 5–10 mm/day over northern areas of lower and central IGP while 3–6 mm/day over the rest of the IGP region (Fig. 3ii(e)). Following other models, RegCM_NOR also shows higher dry bias in the range of − 2 to − 3 mm/day or more over lower IGP. Contrary to other members, a scattered dry bias pattern can be noticed over some central and upper IGP regions (Fig. 3iii(e)). The overall analysis suggests that among all the considered RegCM4.7 simulations, RegCM_EIN75 and RegCM_MPI have shown the least bias over the lower IGP regions, whereas RegCM_MIROC and RegCM_NOR have reported the least bias over central IGP. Further, the performance of RegCM_EIN75, followed by RegCM_MPI, is more realistic in simulating the mean seasonal rainfall over IGP during the historical period.

3.2 Category-wise distribution of extreme rainfall events over IGP

The PDF distribution of observed (IMD) and RegCM4.7 simulated different category rainfall events during the historical period has been shown in Fig. 4a–d. The observed
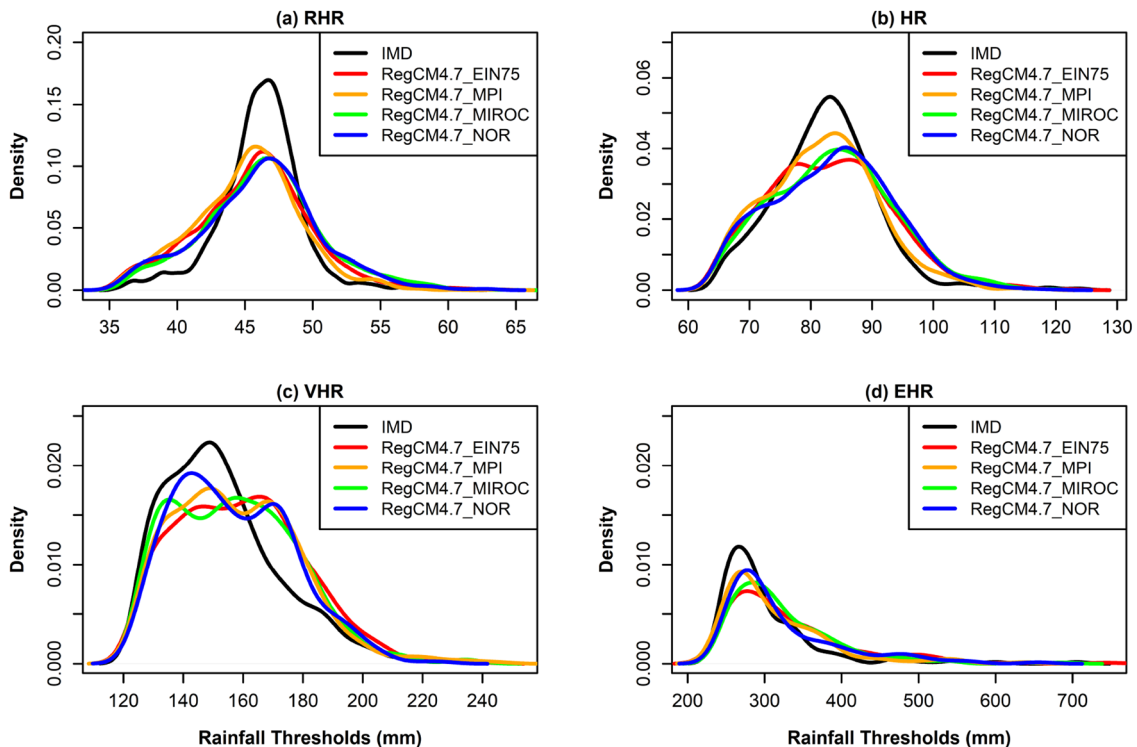

Fig. 4 Distribution of probability density function (PDF) of observed (IMD) and RegCM4.7 simulated (with four forcing) different category rainfall events viz. **a** RHR, **b** HR, **c** VHR, and **d** EHR over IGP during the historical period (1986–2005) at 95% confidence level

RHR depicts that the rainfall of around 44–49 mm in a day is most probably over the IGP region during the ISM season (Fig. 4a). However, the distribution peak is slightly less in all the RegCM4.7 simulations. Still, each follows the distribution pattern precisely as compared to the observations. Similarly, for the HR events category, observations depicting nearly 78–93 mm rainfall days are most probable during the historical period (Fig. 4b). All the RegCM4.7 experiments follow the HR distribution pattern satisfactorily with a slightly less density peak, same as in the case of RHR. RegCM_MPI shows better performance among all the simulations, followed by RegCM_MIROC. For the VHR events, the observation shows maximum rainfall to likely occur within the approximate range from 140 to 170 mm over IGP, and is satisfactorily represented in all of the RegCM4.7 experiments with some irregular pattern around the peak of the distribution (Fig. 4c). All the considered models show a slightly lower peak in the distribution pattern of VHR events compared to observations. Therefore, the RegCM_MPI, RegCM_MIROC, and RegCM_NOR experiments have shown more realistic patterns. Further, the distribution of the most affecting category rainfall events, i.e., the EHR events, is illustrated in Fig. 4d. Observation shows most of the events within the range of 250–320 mm, along with the highest peak around 270 mm over IGP. However, all the models have satisfactorily represented the distribution patterns like observations with slightly lesser peaks. Among all the RegCM simulations, the performance of RegCM_MPI, RegCM_MIROC, and RegCM_NOR show a more realistic distribution pattern in simulating EHR events over IGP. It can be noticed that moving towards the EHR category from the HR category, the performance of RegCM_MIROC and RegCM_NOR improves.

The distribution of different categorized rainfall events during the historical period has been illustrated in Fig. 5a–d. The spatial distribution of observed RHR depicts 69–108 events over most of the central and lower IGP regions, whereas 30–40 events over upper IGP regions during the historical period (Fig. 5a(i)). However, most lower IGP regions have reported 108–121 or more RHR events. The RegCM_EIN75 simulation shows 69–108 events over most of the central and lower IGP regions while 30–43 events over the upper IGP which agree with the observations (Fig. 5a(ii)). RegCM_MPI shows a similar pattern as that of RegCM_EIN75 over the entire IGP except for some southern central IGP regions where ~ 43 events can be noticed (Fig. 5a(iii)). In Fig. 5a(iv), the member RegCM_MIROC also shows a similar distribution as that of RegCM_EIN75 over some northern regions of central and lower IGP as it shows 108–121 numbers of RHR events. Still, its performance is not up to the mark of other IGP regions. Further, the upper

IGP and southern regions of central and lower IGP depicted 30 or fewer events during the period. Similarly, RegCM_NOR shows 32–82 events over a few northern central and lower IGP, whereas an underestimation (30 or less) can be noticed over almost the entire IGP (Fig. 5a(v)). The overall analysis suggests that among all the considered RegCM4.7 simulations, RegCM_EIN75 and RegCM_MPI have performed satisfactorily in simulating the RHR events over the IGP region during the historical period. The distribution of HR events over IGP has been depicted in Fig. 5b(i–v). IMD observations show that the entire IGP reported 32–53 HR events (Fig. 5b(i)). However, a few upper IGP regions show fewer events in the 30–43. The model RegCM_EIN75 underestimates the number of events (30–43) over upper IGP, but its performance is satisfactory over central and lower IGP regions (Fig. 5b(ii)). The RegCM_MPI shows a close pattern to RegCM_EIN75 over the entire IGP region. It also depicts improved distribution (closer to the observation) compared to the RegCM_EIN75 by reporting up to 18 events over lower IGP regions. The member RegCM_MIROC also shows a similar pattern as RegCM_EIN75 and RegCM_MPI with an underestimation (> 4 events) over southern regions of lower IGP. Similarly, the RegCM_NOR has performed satisfactorily over some northern central and lower IGP regions, while its performance is not satisfactory over other IGP regions. The overall analysis suggests that RegCM4.7 has performed satisfactorily in all the downscaling experiments where the RegCM_MPI is more realistic. The distribution pattern of observed VHR events shows 0–11 events during the historical period (Fig. 5c(i)). Most lower IGP and northern central and upper IGP regions have shown 7–11 events, while southern regions reported 1–3 or fewer events. Regarding modeling aspects, the RegCM_EIN75 performs poorly in simulating VHR events over almost the entire IGP region, as it can reproduce 3–7 events over only a few northern regions (Fig. 5c(ii)). RegCM_MPI and RegCM_MIROC simulations have shown similar but improved performance over the entire IGP compared to the RegCM_EIN75 but with some underestimation (Fig. 5c(iii–iv)). They have shown 7–11 events over northern IGP regions which agree with the observations. However, RegCM_MPI has shown more realistic results (5–9 events) than the RegCM_MIROC (< 3 events) over southern lower IGP regions. The downscaling experiment with RegCM_NOR performed poorly over the entire IGP. The overall analysis suggests that RegCM_MPI followed by RegCM_MIROC have simulated the VHR events satisfactorily over the IGP region. Further, the EHR categorial events can be illustrated in Fig. 5d(i–v). The maximum number of EHR events (3–4 or more) has been reported over the northeastern lower IGP as compared to the rest of the IGP region (Fig. 5d(i)). There are also some
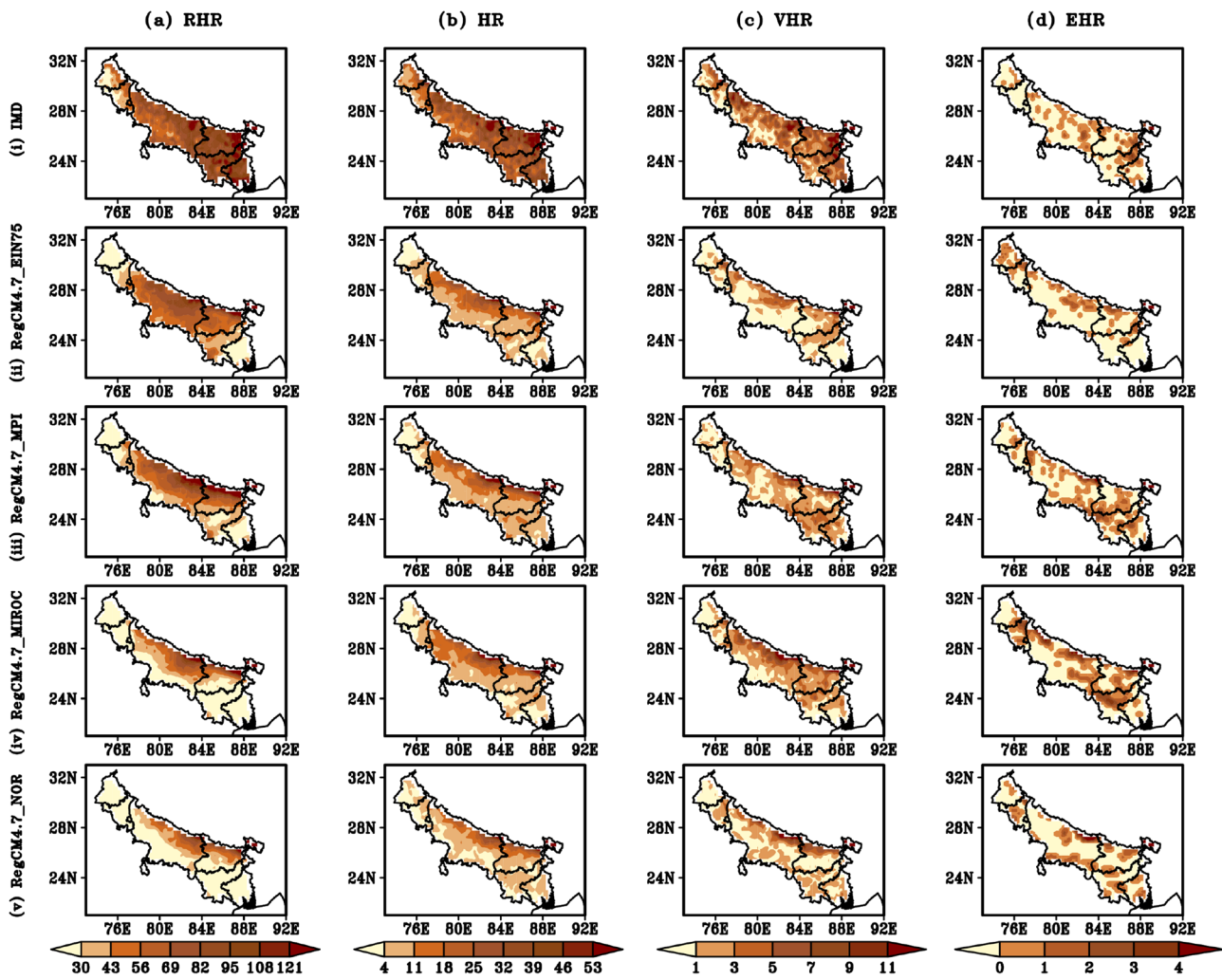
Fig. 5 The spatial distribution of **i** observed IMD, **ii** RegCM4.7_EIN75, **iii** RegCM4.7_MPI, **iv** RegCM4.7_MIROC, and **v** RegCM4.7_NOR simulated rainfall with different categorical events viz. **a** RHR, **b** HR, **c** VHR, **d** EHR over IGP during the historical period of 1986–2005

isolated regions over the upper, central, and lower IGP where 2–3 events have been reported. In contrast, most regions reported one or none of the EHR events during the period. The RegCM_EIN75 shows an underestimation (1 or no events) over lower and central IGP. In contrast, it has shown an overestimation (1–2 events) in simulating the number of EHR events over the upper IGP region (Fig. 5d(ii)). The RegCM_MPI performs reasonably well over the entire IGP and produces more realistic results when compared with observations (Fig. 5d(iii)). However, it depicts some overestimation (1–2 events) over southern areas of the central and lower IGP region. The performance of RegCM_MPI in simulating EHR events over IGP is excellent so far. However, some locations or scaling errors are needed future attention. Similarly, RegCM_MIROC performs finely over the entire

IGP as the RegCM_MPI does, but it shows overestimated EHR events over upper IGP and southern areas of lower IGP (Fig. 5d(iv)). The RegCM_NOR also performs satisfactorily but with the least skill compared to other considered simulations (Fig. 5d(v)). Dash et al. (2009) studied the long-term characteristics of different category rainfall events. However, they found some different results than this study. They concluded by discussing a decreasing trend in moderate rainfall events whereas an increasing trend in heavy to very heavy rainfall events over the central northeast region of India (which exhibits a large area of IGP). The overall analysis suggests that RegCM4.7 simulations, RegCM_MPI followed by RegCM_MIROC and RegCM_EIN75 show better skill in simulating all category rainfall events over IGP during the historical period. Further, it can be noticed that

Table 3 Mean thresholds for different category rainfall events (mm/day) during the historical period (1986–2005) over IGP

	RHR	HR	VHR	EHR
IMD	46.6	83.4	156.8	308
RegCM_EIN75	45.6	81.3	162.2	344.3
RegCM_MPI	45.5	82.1	165.5	351
RegCM_MIROC	45.7	85.1	164.7	358.3
RegCM_NOR	45.8	84.4	160.9	357.0

as moving from HR events to the EHR category, the performance of RegCM_MIROC gets improved, whereas at the same time skill of RegCM_EIN75 deteriorates. Further, the mean thresholds for different category rainfall events have been listed in Table 3. The IMD observations have reported thresholds for various category rainfall events over IGP as 46.6 mm (RHR), 83.4 mm (HR), 156.8 mm (VHR), and 308 mm (EHR) during the historical period. The downscale simulation efficiently captures the RHR rainfall events ranging from 45.5 to 45.8, the HR events ranging from 81.3 to 85.1, and the VHR rainfall events ranging from 160.9 to 164.7. However, an overestimation in simulating the EHR threshold can be noticed in all the RegCM4.7 simulations. The range lies between 344.3 and 358.3 in the event. The RegCM4.7 downscaling experiments underestimate most rainfall events under RHR and HR and overestimate the categorized extreme events with VHR and EHR.

3.3 Projected future changes in patterns of rainfall and associated extremes under the warming scenario

3.3.1 Projected rainfall patterns and relative changes in NF and FF

The projected annual cycle of average rainfall under the RCP8.5 scenario and the associated relative changes w.r.t. the historical period over IGP is considered during the NF and FF with different RegCM4.7 experiments (Fig. 6). The rainfall pattern during NF suggests that all the simulations follow a similar pattern (Fig. 6a). The RegCM_MPI and RegCM_MIROC have projected maximum rainfall around 10 mm/day during July–August. In comparison, RegCM_NOR has shown its peak around 7 mm/day. A shifted pattern in maximum rainfall during the year (i.e., monsoon rainfall) can be seen in Fig. 6b, where 40% or more declines during June across all the model experiments (Dash et al. 2009; Mishra et al. 2016; Mukherjee et al. 2018) (Fig. 6c). In addition, an increase (40–80%) in rainfall from July to November over IGP has been projected in NF. The projected rainfall pattern during FF shows that RegCM_MPI, the best-performing model so far, depicts maximum rainfall during the July to November months with peak rainfall of ~ 10 mm/day during September (Fig. 6d). The other simulations, RegCM_MIROC and RegCM_NOR, also depict a similar pattern as that of RegCM_MPI but with a smaller
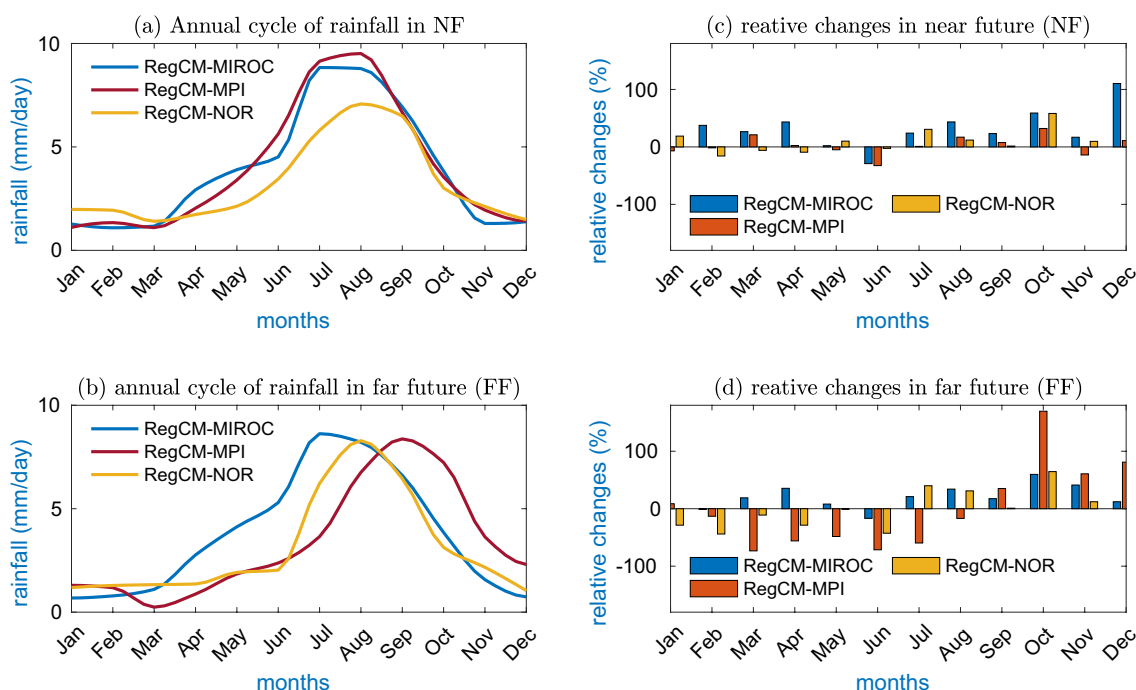

Fig. 6 The RegCM4.7 projected **a**, **b** annual cycle of rainfall (mm/day) under RCP8.5 scenario during **a** near future (NF; 2041–2060) and **b** far future (FF; 2080–2099). **c, d** The relative changes (%) in rainfall during **c** NF, and **d** FF w.r.t. the historical period (1986–2005)

shift in maximum rainfall months towards later months of the year. The changes in rainfall pattern during FF suggest a decline in rainfall from 40 to 80% during the March to August months which includes the 3 months of ISM season, whereas an increase of 50–100% can be noticed during the September, October, November, and December months of the year. It is to be noted that a huge enhancement of around 170% in rainfall may occur during October in FF. The above discussion suggests that there may be a shift in the monsoon regime towards the later months of the year, along with the significant decline in rainfall during JJAS and pre-monsoon months. These results also agree with the study of Shahi et al. (2021) on India and MCR. It is further supported by the recent work of Ashfaq et al. (2021), who have found a delay in South Asian monsoon onset along with the reduction in rainfall during pre-monsoon and monsoon months under high emission RCP8.5 scenario.

The projected relative changes (%) in seasonal mean rainfall over the IGP during the NF and FF compared to the historical period are shown in Fig. 7. The RegCM_MPI projected a ~10 % decline in rainfall over the entire IGP region except for southern areas of central IGP where ~ 20% of the decrease in rainfall can be noticed during NF

(Fig. 7a(i)). RegCM_MIROC projected a ~ 10% increase over upper and central IGP regions, whereas a moderate decrease of 10–20% in seasonal rainfall has been reported over lower IGP regions during NF (Fig. 7a(ii)). Similarly, the RegCM_NOR projections show a decline of ~ 20% or more in seasonal rainfall over almost the entire IGP except for a few extreme lower and upper IGP regions, where it depicts a moderate enhancement of nearly ~ 10% in average ISM rainfall during NF. Figure 7b(i–iii) represents the projected relative changes with historical periods in ISM rainfall during FF. The model RegCM_MPI shows a maximum decrease in precipitation (30% or more) over almost the entire IGP region except for a few lower IGP regions where a 10–20% of decline in rainfall noticed in comparison to the historical period has been projected during the ISM season (Fig. 7b(i)). The RegCM_MIROC projects a maximum decline (30% or more) over only some isolated regions of upper IGP while a moderate decrease (~ 10%) over the rest of the IGP regions during the FF (Fig. 7b(ii)). Also, a nearly 20–30% increase can be noticed over southern lower IGP regions. The RegCM_NOR has projected a 20–30% rise in seasonal rainfall over upper IGP while a moderate to higher decline (10–20%) over central IGP regions
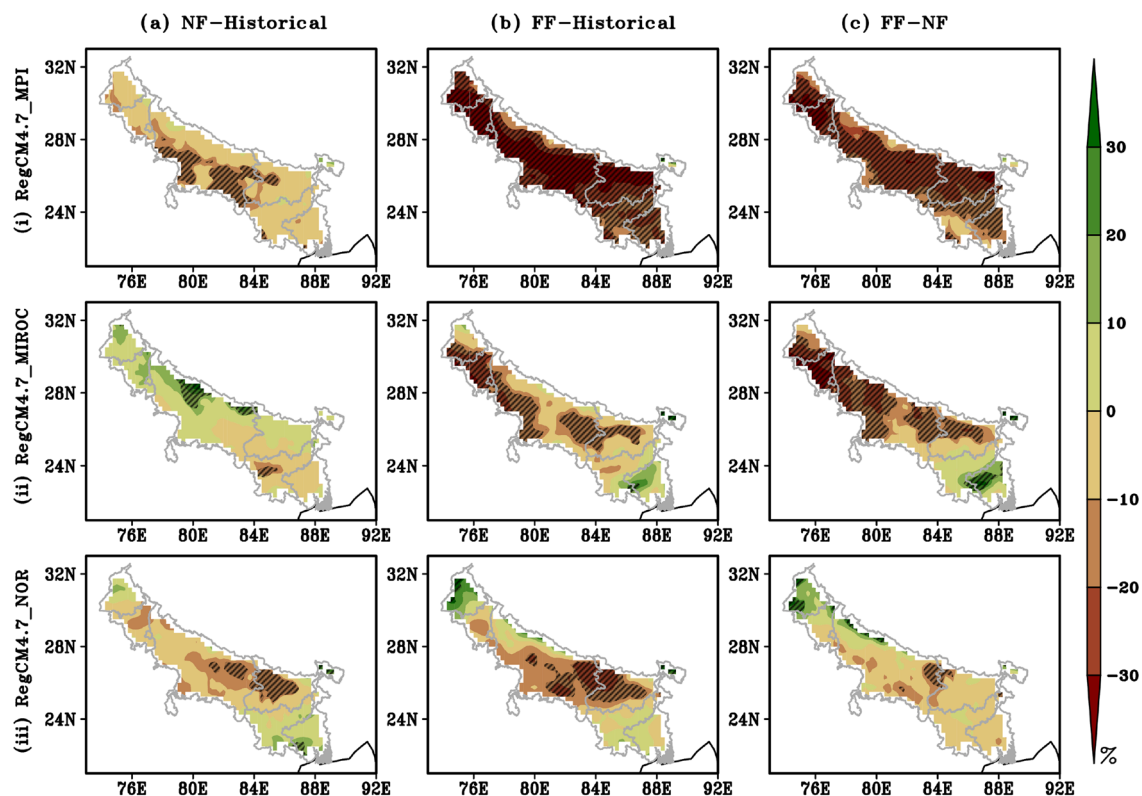
Fig. 7 RegCM4.7 Projected relative changes (%) of mean monsoon seasonal rainfall under the RCP8.5 scenario over the IGP region during **a** Near future (NF; 2041–2060) and **b** Far future (FF; 2080–2099) compared to the historical period (1986–2005). **c** Changes in FF compared to the NF. The model simulations with four different GCM forcings are represented as **i** RegCM_MPI, **ii** RegCM_MIROC, and **iii** RegCM_NOR. The hatched region shows data distribution at 99% confidence level

(Fig. 7b(iii)). Further, a slight enhancement in seasonal rainfall can be noticed over lower IGP regions during FF relative to the historical period. Figure 7c depicts the projected relative changes in mean ISM rainfall during FF and NF. The RegCM_MPI suggests a decrease (10–30%) in rainfall over almost the entire IGP. However, RegCM_MIROC also projects a similar pattern as that of RegCM_MPI over the upper IGP regions. Still, it shows a moderate to higher seasonal rainfall increase (10–30%) over lower IGP regions. Contrary to other experiments, the RegCM_NOR has projected a 20–30% rise over upper IGP. At the same time, it shows a slight decline in seasonal rainfall over central and lower IGP regions during FF compared to NF. The decline in seasonal monsoon rainfall over IGP can be attributed to the increased atmospheric aerosols (Bollasina et al. 2011). According to student's t statistics, the changes over hatched regions during future time scales are significant at a 99% confidence level. The overall analysis suggests that RegCM4.7 has projected a moderate to higher decline in mean ISM rainfall over the IGP region under the high-emission RCP8.5 scenario. The above discussion also agrees with the study of Maharana et al. (2020), who also found a decrease in mean rainfall over IGP regions under a warming climate.

3.3.2 Projected changes in the category-wise distribution of extreme rainfall events

The PDF distribution for the different categorized projected rainfall events under the RCP8.5 scenario over IGP during NF and FF periods are illustrated in Fig. 8. The distribution of RHR depicts that all the three experiments have shown similar distribution patterns during NF as well FF (Fig. 8a(i, ii)). However, RegCM_MPI and RegCM_MIROC show higher peaks than RegCM_NOR, which are identical to the historical period. Also, the distribution shows 43–50 mm/ day rainfall days are most probable during NF and FF. Similarly, the HR events distribution depicts that most days fall under 80–98 mm/day rainfall, and RegCM_MPI, followed by RegCM_MIROC, shows the highest peak among all data sets (Fig. 8b(i, ii)). Further, it can be noticed that the distribution of HR events suggests an increasing shift in rainfall intensity during the NF and FF periods as compared with historical periods. Figure 8c(i, ii)) shows the projected distribution of other category rainfall events, i.e., VHR events over IGP in NF and FF. It can be noticed that the events, when 140–190 mm of rainfall occurs in a day, are most probable during both the time slices (NF and FF). Further, all the models have projected the highest peak for the rainfall events when 180 mm (during NF) or more (during FF) in a day might occur, which is much higher than the historical period (nearly 150 mm). Similarly, all models have shown similar patterns in projecting the probability density distribution of EHR events during the NF and FF periods. However,

among all the RegCM4.7 simulations, RegCM_MPI shows a maximum peak during both time slices. The distribution of EHR events shows that the days when rainfall ranging from 250–350 mm is reported are most probable, along with peaks of nearly 300 mm or more during the NF and FF. Further, it can be noticed that the maximum rainfall limits may enhance in the future as the probability density distribution shows maximum rainfall up to 800 mm and 900 mm in a day during NF and FF, respectively, as compared with the historical limit, i.e., 700 mm. These results indicate extreme intensification under warming scenarios in the future.

The RegCM4.7 projected (under RCP8.5 scenario) changes in the number of different category extreme rainfall events over IGP during the NF and FF compared with historical periods has been shown in Figs. 9 and 10, respectively. RegCM_MPI has projected an increase of 15–20 in RHR over most of the lower IGP and a few regions of upper IGP (Fig. 9a(i)). A slight decrease (5 or less) over central IGP and northern areas of lower IGP during NF has been projected. The RegCM_MIROC has also projected increased RHR events over lower and IGP regions. Still, it shows an exceptional enhancement (20 or more events) over northern areas of central and upper IGP (Fig. 9a(ii)). However, a decrease (5 or less) can be noticed over the central IGP region. The RegCM_NOR has shown a slight increase (0–15) over upper and most lower IGP regions in projecting the number of RHR events during NF compared with the historical period. The distribution pattern of projected changes in the number of HR events during NF has been illustrated in Fig. 9b(i–iii). It can be seen that RegCM_MPI has projected an increase in the number of HR events ranging from 3 to 15 or more over the entire IGP region except for a few northern areas of central and lower IGP, where it reports a slight decrease during NF (Fig. 9b(i)). The RegCM_MIROC shows a slight increase and decline over lower and upper IGP, whereas it projects potential enhancement (~ 15 HR events) over northern regions of central IGP in NF (Fig. 9b(ii)). Similarly, the RegCM_NOR depicts the pattern as that of RegCM_MIROC but with very slight changes (increase/decrease) in the number of HR events over the entire IGP in NF (Fig. 9b(iii)). The RegCM_MPI projected changes in the following category rainfall events, i.e., VHR events show moderate to higher enhancement (5–10) over most of the IGP except a few lower IGP regions where a slight decrease (5 or less) can be noticed during NF (Fig. 9c(i)). Both RegCM_MIROC and RegCM_NOR show almost similar patterns over upper and central IGP regions where a combination of slight increase/decrease (5 or less) has been projected during NF (Fig. 9c(ii, iii)). However, RegCM_MIROC shows a pattern, while RegCM_NOR shows a slight enhancement in VHR events over some lower IGP regions during NF. The projected changes in the most disastrous category rainfall events, i.e., the EHR events, are illustrated in Fig. 9d(i–iii).
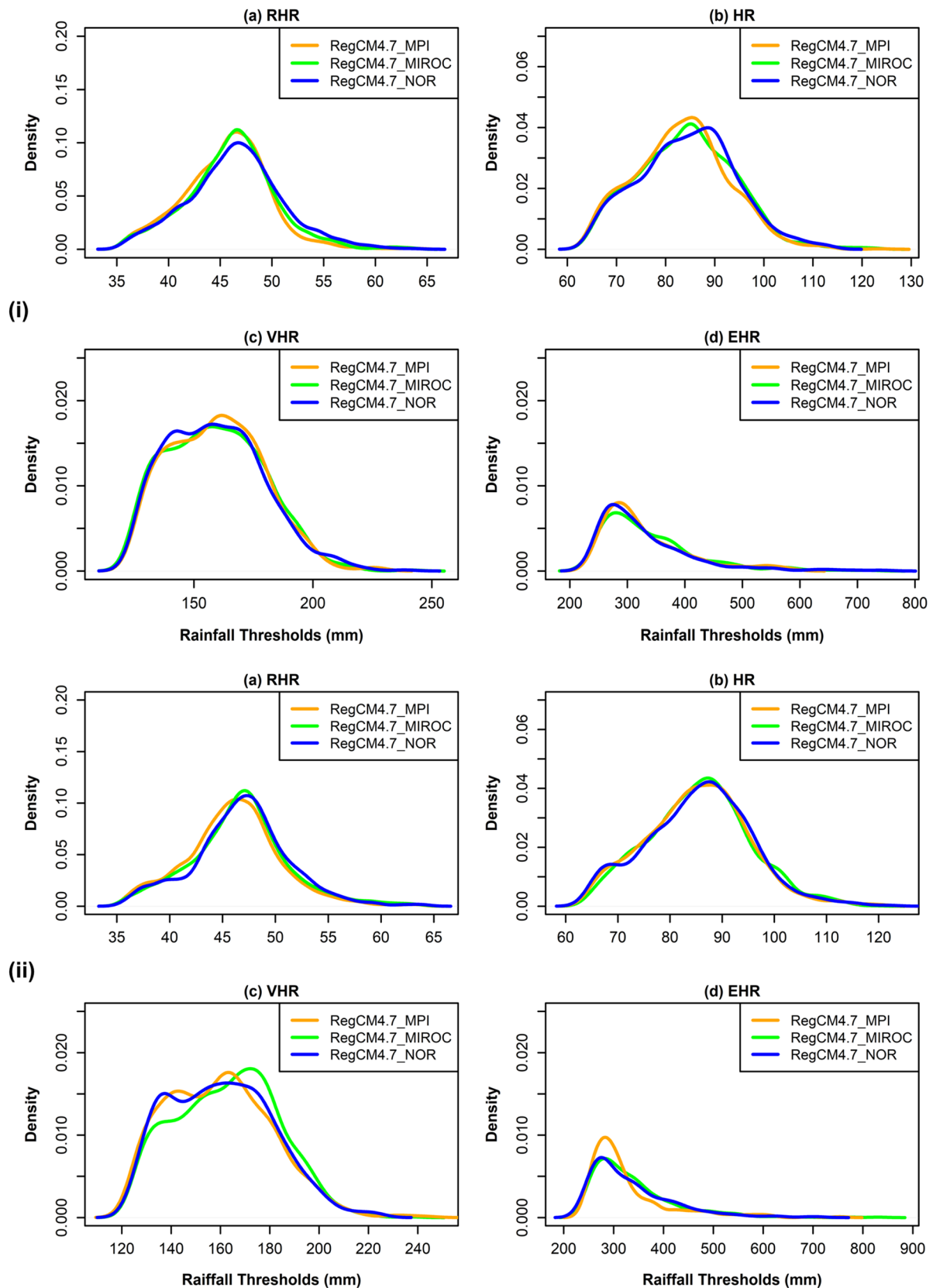
Fig. 8 Same as Fig. 4 but for [**i**(**a–d**)] Near future (NF; 2041–2060) and [**ii**(**a–d**)] Far future (FF; 2080–2099) periods. Distribution is considered at 95% confidence level
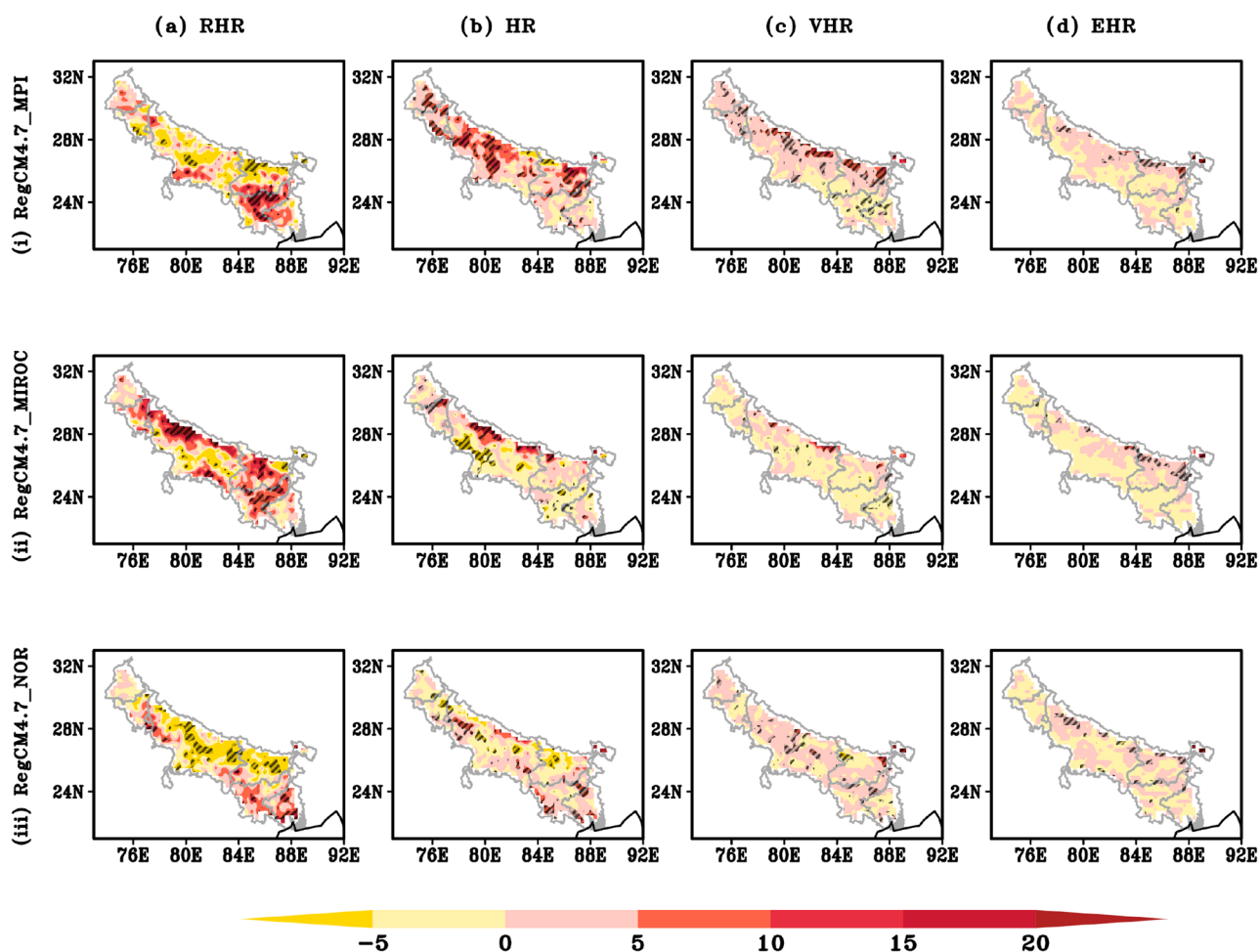
Fig. 9 The spatial distribution of RegCM4.7 projected changes under the RCP8.5 scenario in numbers of different category rainfall events viz. **a** RHR, **b** HR, **c** VHR, and **d** EHR over IGP during Near future (NF; 2041–2060) as compared with the historical period (1986– 2005). The model simulations with four different GCM forcings are represented as **i** RegCM_MPI, **ii** RegCM_MIROC, and **iii** RegCM_ NOR. The hatched regions represent the data distribution at a 90% confidence level

The RegCM_MPI depicts a maximum enhancement of 5 or more EHR events over extreme northern regions of the entire IGP, whereas a slight decrease of 1 or more over southern IGP regions. Further, over the rest of the IGP, it shows an increase (5 or less) in the number of EHR events during NF. The member RegCM_MIROC (Fig. 9d(ii)) also projects a similar EHR distribution as that of RegCM_MPI over almost the entire IGP except for a few southern lower and central IGP regions where a decline of one or more has been projected. At last, the model RegCM_NOR projects a scattered distribution of slight increase and decrease in EHR events over the entire IGP region. However, an increase of 5 or more events can be noticed over some northern lower IGP regions. The results indicate an increase in extreme rainfall events (specifically higher rainfall category) over IGP and a slight decrease in moderate to higher rainfall category events. These results are in accordance with the findings of Ali et al. (2014); Dash et al. (2009); Roxy et al. (2017),

who have proposed an increase in rainfall extremes and a decrease in 75th (i.e., moderate) rainfall events over India.

The projected changes in the number of different category rainfall events during FF compared to historical periods have shown in (Fig. 10a–d). The RegCM_MPI projected changes show a decline of > 5 in RHR over the entire IGP. However, an increase of 5–20 can be noticed over southern lower and northern upper IGP regions (Fig. 10a(i)). The RegCM_ MIROC has projected 10–20 or more increments in the number of RHR events over lower IGP while a scattered distribution of slight increase and decrease over the rest of the IGP regions (Fig. 10a(ii)). Similarly, RegCM_NOR also depicts a similar pattern as earlier discussed models, but changes are slightly less (Fig. 10a(iii)). Overall, a decline in RHR can be noticed over the entire IGP in FF as compared to the NF (Fig. 9) during ISM season, which can also be explained per the study of Pattanaik and Rajeevan (2010), where they have found a significant decreasing trend in the frequency
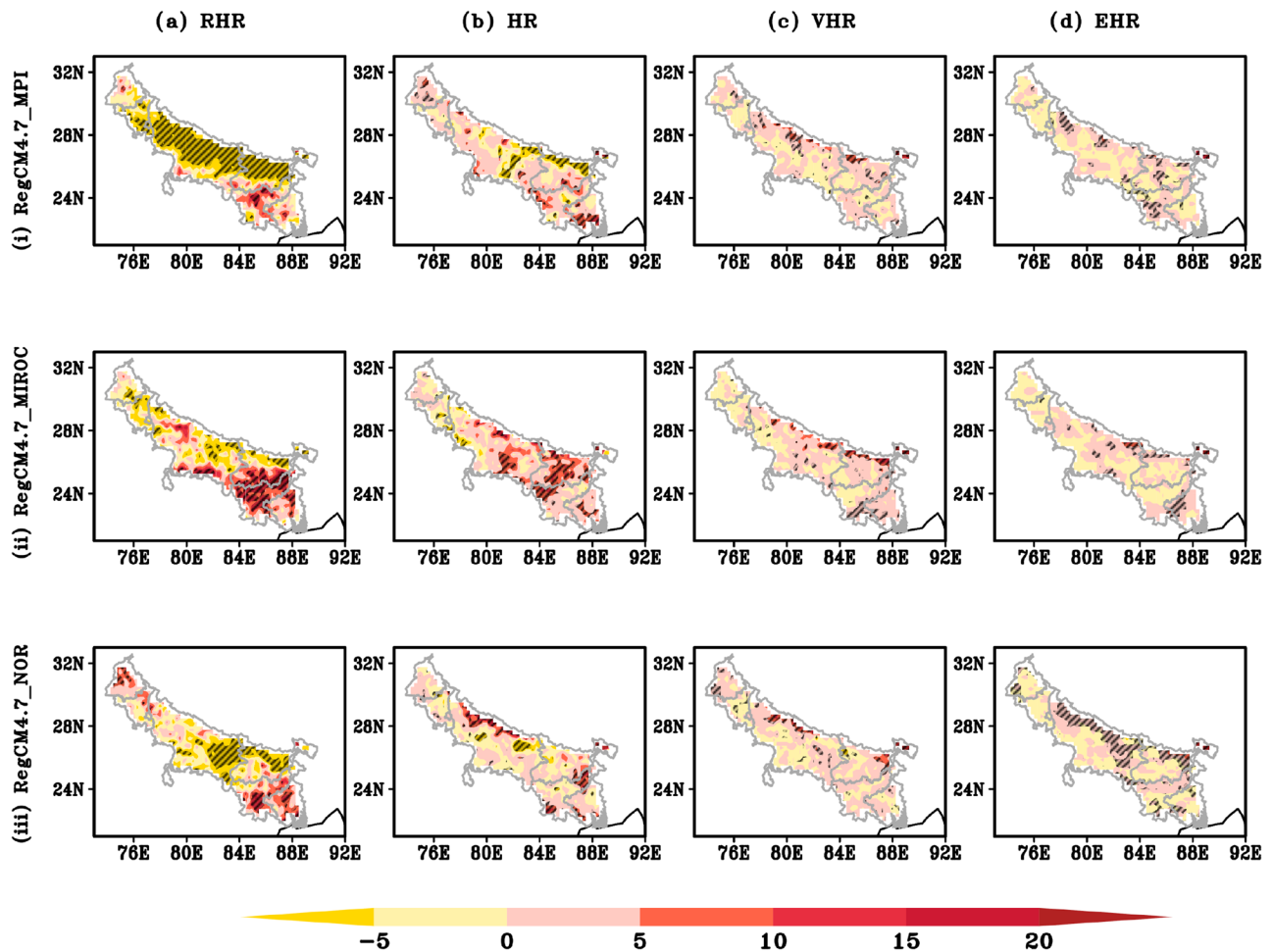
Fig. 10 Same as Fig. 9 but for the Far Future (FF; 2080–2099)

of RHR events. The RegCM_MPI projected changes in HR events also depict slight decreases (5 or fewer events) over central and a few northern regions of lower IGP. However, an increase (5–15 occurrences) can be seen over lower and upper IGP during FF compared to the historical period (Fig. 10b(i)). The member RegCM_MIROC has projected an enhancement (5–15) over central and lower IGP while a decrease for 5 or more HR events over upper IGP during FF, contrary to the NF projections. The RegCM_NOR shows a combination of slight increase and decrease ~5 events in HR events throughout the IGP region along with potential enhancement of 5–15 occurrences over some northern areas of central and lower IGP. Therefore, RegCM_NOR projects a similar pattern during FF as shown for the NF period. The distribution of RegCM_MPI projected VHR events depicts moderate to higher enhancement (∼ 5 events) over the entire IGP except for very few southern lower IGP regions where a slight decline of 5 or fewer events can be noticed during FF (Fig. 10c(i)). However, the changes are slightly less than NF (refer to Fig. 9). Other models RegCM_MIROC

and RegCM_NOR, have projected an increase of 5 to 10 events over the entire IGP during FF. Some isolated regions can also notice a slight decrease (5 or less). Further, both models have projected a slight enhancement in VHR events during FF compared to NF. Similarly, the figure (Fig. 10d(i)) represents RegCM4.7 projected changes in EHR events during FF. It can be noticed that changes are similar for all the considered models as that during NF (refer to Fig. 9d). All three of the RegCM projections have shown moderate to higher increases (1–5) in EHR events over the entire IGP except few lower IGP regions. The increase in the number of events is most prominent over northern IGP regions. The overall analysis suggests that all the models have shown similar patterns in projecting different category rainfall events over IGP in NF and FF during ISM season compared to the historical period. Further, it can be noticed that the increase in events is more significant during NF than FF, and the decrease in events is more prominent during FF than NF during JJAS or ISM season. It may be because the ISM season is shifting towards later months of the year, and there is a

decline in rainfall during the ISM season months, namely, June, July, and August in NF and FF (refer to Fig. 6). The hatched regions in Figs. 9 and 10 are showing the regions with significant changes (90% confidence level) in different category rainfall events during NF and FF.

The RegCM projected relative changes (%) under the RCP8.5 scenario in mean thresholds for different category rainfall events have shown in Table 4. The changes for RHR events are significantly less < than 1% (either increase or decrease) during NF and FF compared to historical periods in all three model projections. The RegCM_MPI projects a 2.2% rise in HR threshold during NF while it shows further enhancement (∼ 3%) during FF. Contrary to that, the rest of the RegCM4.7 experiments have projected a slight to moderate decrease during NF (2.5% in RegCM_MIROC and 0.16% in RegCM_NOR) and FF (0.5% in RegCM_MIROC and 0.11% in RegCM_NOR) as compared to the historical period. In the case of VHR events, the RegCM_MPI projection shows a 2.4% decline during NF while only a 0.2% decline during FF. Further, the member RegCM_MIROC also indicates a decrease of ∼ 1.7% in mean VHR thresholds during NF, whereas it shows a slight increase (0.7%) during FF. Similarly, the RegCM_NOR projects a slight increase of 1.5% and 1.8% in the VHR threshold during NF and FF, respectively. The thresholds for the most disastrous rainfall events, i.e., EHR, found an increase by all RegCM4.7 experiments during both the future time slices. It can be noticed that the models RegCM_MPI, RegCM_MIROC, and RegCM_NOR have projected 4.9%, 7.7%, and 0.97%, increase during NF while 1.95%, 4.28%, and 2.33%, respectively of increase during FF in mean EHR thresholds. It can be noticed that the RegCM projects massive enhancement in the mean threshold of EHR events during NF and FF, which may be an indication that extremes are getting intensified under a warming climate (Mukherjee et al. 2018; Roxy et al. 2017). However, the changes are slightly less during FF than NF, which is explained in the earlier section that there may be a shift in ISM seasonal rainfall towards later months of the year under warming scenarios.

Table 4 Relative changes (%) in mean thresholds for different category rainfall events over IGP during NF and FF as compared with the historical period

	Model	RHR	HR	VHR	EHR
NF-Hist	RegCM_MPI	0.8	2.2	− 2.4	4.9
	RegCM_MIROC	− 0.4	− 2.5	− 1.7	7.7
	RegCM_NOR	− 0.2	− 0.16	1.5	0.97
FF-Hist	RegCM_MPI	1	3	− 0.2	1.95
	RegCM_MIROC	0.65	− 0.59	0.7	4.28
	RegCM_NOR	0.65	− 0.1	1.8	2.33

4 Discussion

Global warming has imposed its effects on the rainfall patterns as the mean precipitation is anticipated to decrease while heavy rainfall events are increased (Tabari 2020). Therefore, examining the behavior and response of different climate components (dynamical and thermodynamic) during extreme rainfall is necessary. For that purpose, here we have shown the anomalous patterns of RegCM_MPI simulated (which is the best-performing member so far) tropospheric TG, hus, and MSLP (superimposed with the wind, i.e., u &v at 850 hPa) over the region of interest during historical as well as future time slices (Figs. 11, 12). The temporal evolution of earlier mentioned quantities/variables during the historical period has been presented in (Fig. 11). The Lead4, Lead2, and Lag1 represent the patterns 4 days before, two days before, and one day before the day of the extreme rainfall event (Lag0), respectively. The beginning of positive TG build-up over central and lower IGP region (0.5–1 °C) can be seen in Lead4 (Fig. 11i(a)), which gets enhanced (∼ 1.5 °C) gradually up to Lead1 (Fig. 11i(c)) and gets strongest (2.5–3 °C) on the extreme rainfall day, i.e., Lag0 (Fig. 11i(d)). The TG supports the monsoon onset propagation and advancement mechanism over the Indian region (Ghosh et al. 2022). The distribution pattern of hus is interesting (Fig. 11ii(a–d)). At Lead4, the entire considered domain shows a positive anomalous pattern of hus ranging from 0.4 to 0.8 Kg/Kg, which gets more vital day by day, reaching a maximum of 1.6–2 Kg/Kg on the Lag0. The maximum hus found to be concentrated over central IGP following the earlier discussed TG pattern during the historical period. The dynamical mechanism of rainfall extreme is further supported by the time-dependent evolution of MSLP and wind in Fig. 11iii(a–d) The presence of a low-pressure system (LPS) or convergence zone with negative MSLP anomalies (− 1 to − 1.6 hPa) over the south of the lower IGP can be noticed. This LPS moves northward and gets deeper (− 1.9 to − 2.5 hPa) with time (Lead2) by strengthening of wind (Fig. 11iii(c)). Further, after its intrusion over lower IGP on the day before (Lead1), it stretches and finally settled over the entire IGP, considering the deepest (> 2.5 hPa) over the central IGP region with a more robust cyclonic circulation (Fig. 11iii(d)). The RegCM_MPI simulated evolution mechanism robustly explains the occurrence of extreme rainfall events over IGP, which shows the capability of RegCM4.7 in simulating extreme rainfall characteristics and governing processes over IGP.

In a warming climate scenario, the concentration of water content in the atmosphere increases in proportion to the saturation concentration by increasing the temperature (Trenberth et al. 2003; Stocker 2014). In that view, a
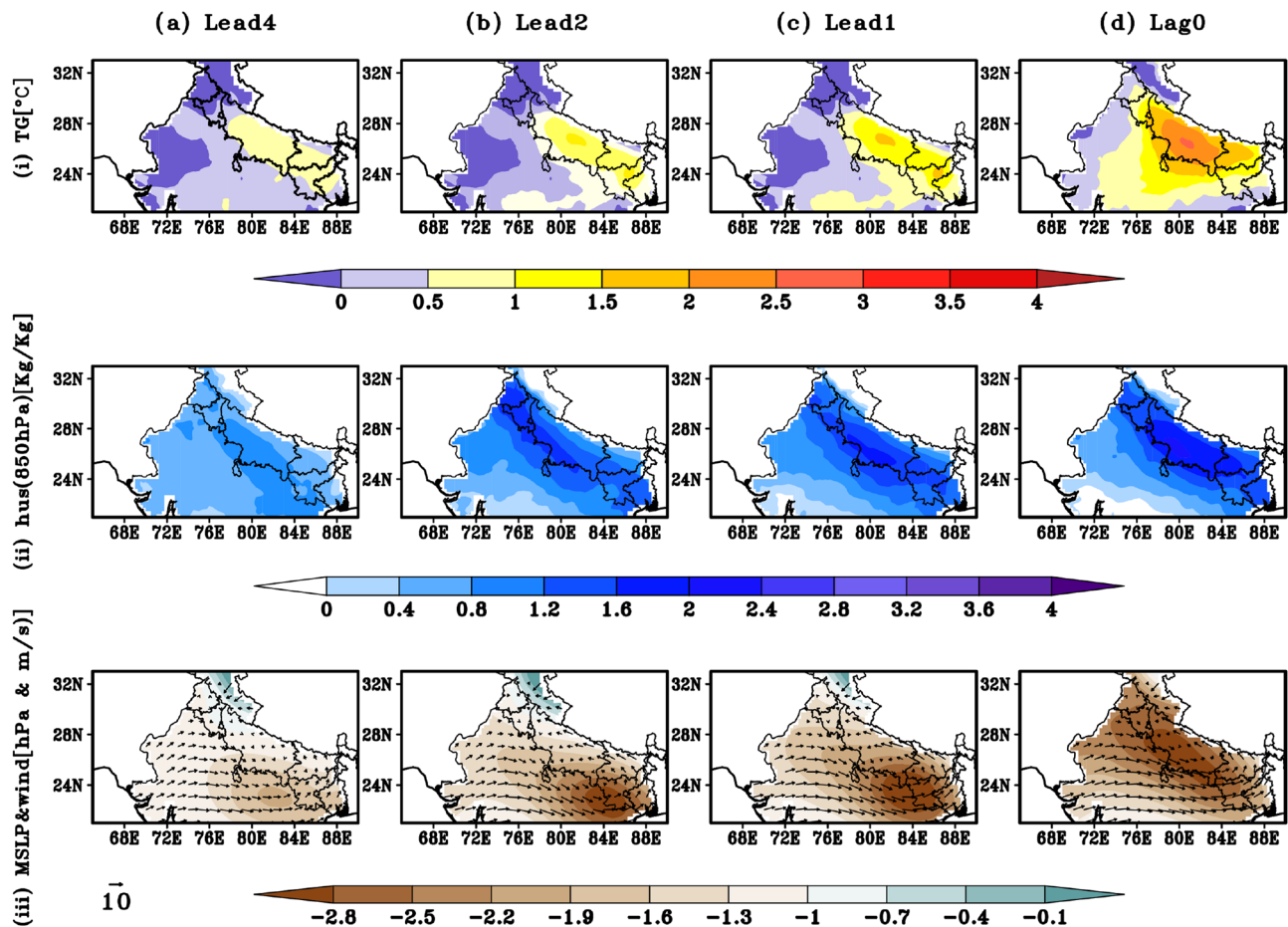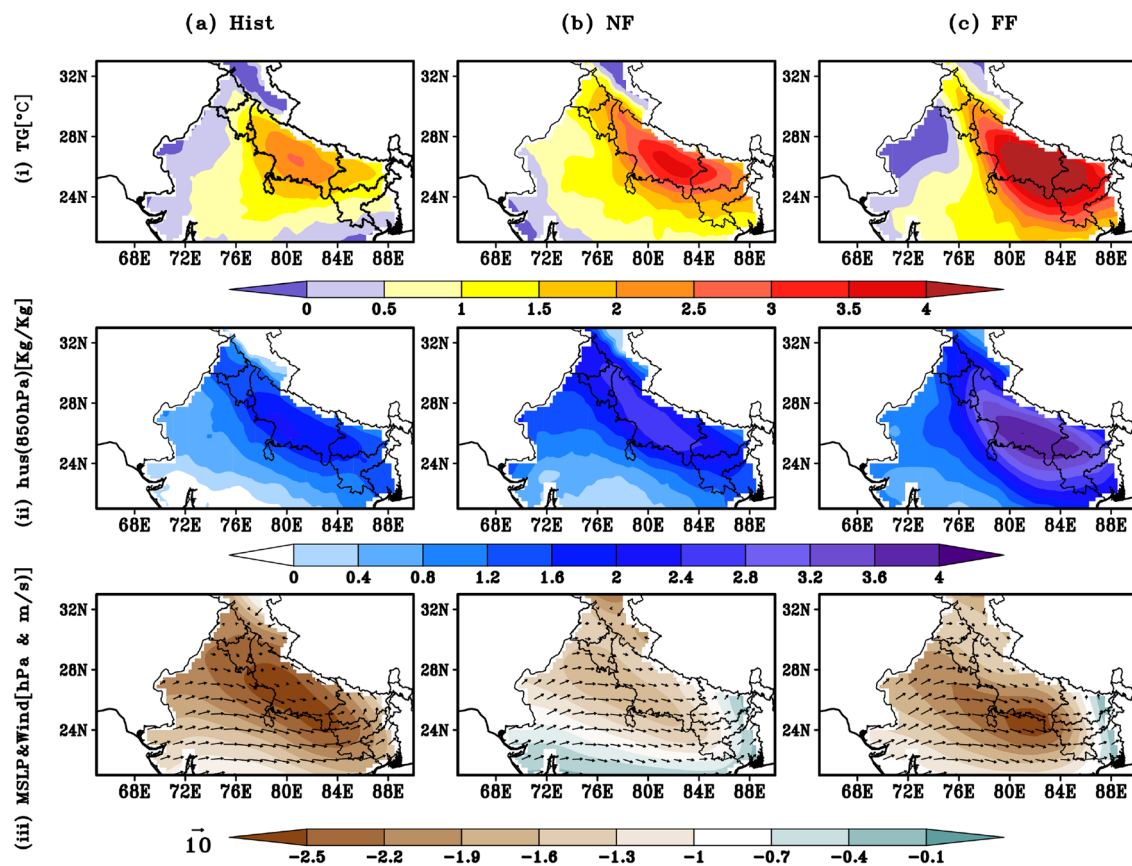
Fig. 11 The composite anomalous spatial distribution of RegCM4.7 simulated **i** TG (°C), **ii** hus (Kg/Kg) at 850 hPa, and **iii** MSLP (hPa) and wind at 850 hPa (u &v; m/s; superimposed considering the vector sign) over IGP during the historical period (1986–2005). The **a** Lead4, **b** Lead2, **c** Lead1, and **d** Lag0 represent the distribution 4 days before, two days before, 1 day before, and the day of the extreme rainfall event, respectively

comparative analysis of earlier discussed dynamical and thermodynamic quantities during historical, NF and FF under high emission RCP8.5 scenarios is considered in Fig. 12. The composites of variables TG, hus, and MSLP with wind on the day of extreme rainfall are discussed. The TG pattern in the historical period can be seen in Fig. 12i(a). It shows a significant enhancement over the entire IGP in NF, where the TG changes by 2–3.5 °C (Fig. 12i(b)). The TG further shows an increase of 3–4 °C or more during FF compared to the historical period (Fig. 12i(c)). The distribution maxima can be seen over the central and lower IGP regions on the event day. Similarly, the anomalous composites of hus show intensified projected patterns in NF and FF (Fig. 12ii(a–c)). The presence of higher moisture content of 2.4–3.2 Kg/Kg can be noticed in NF (Fig. 12ii(b)), while the highest 4 Kg/Kg or more in FF (Fig. 12ii(c)) have been projected over

the IGP region during the extreme rainfall days under high emission RCP8.5 scenario. According to a report on the assessment of climate change over the Indian region, the increased occurrence of rainfall extremes over Indian areas is attributed to changes in moisture content due to the warming caused by GHG emissions, increased urbanization, and aerosol concentrations (Krishnan et al. 2020). Further, the MSLP pattern shows weaker LPS and wind circulation over IGP in future time scales (NF and FF) compared to the historical period (Fig. 12iii(a–c)). Taylor et al. (2012) have also found the weakening of LPS activities over Indian regions in intermodel projections under the RCP8.5 scenario. They found that the decline of troughs during the ISM circulation is compensated by the copious enhancement in atmospheric moisture content, which leads to increased precipitation events over IGP in the future.

Fig. 12 The composite anomalous spatial distribution of RegCM4.7 simulated **i** TG (°C), **ii** hus (Kg/Kg) at 850 hPa, and **iii** MSLP (hPa) with wind (u &v) in m/s at 850 hPa over IGP during the **a** historical period (Hist; 1986–2005), **b** near future (NF; 2041–2060) and **c** far future (FF; 2080–2099)

5 Conclusions

This work has been attributed to assessing the spatial and temporal variability in ISMR and associated extremes over IGP using RegCM4.7 during the past and future time slices (NF and FF) under the RCP8.5 scenario. The dynamically downscaled RegCM4.7 with different reanalysis and GCM forcings perform well in simulating the rainfall characteristics over the IGP region during ISM season. However, RegCM4.7 with EIN75 and MPI-ESM-MR forcing offers better performance among all the considered RegCM4.7 simulations. The annual mean rainfall cycle is well represented in all the RegCM4.7 simulations. Future projections suggested a 10–20% significant decline in mean ISMR with a massive decrease during the earlier ISM seasonal months (i.e., June and July) in NF compared to the historical period. Further, a considerable decline (< 30%) in mean JJAS rainfall along with a 40–70% decline during June–July months, and an abrupt increase of 80–170% during the post-monsoon months (i.e., October, November, and December) is projected under the RCP8.5 scenario.

The decline in rainfall during JJAS and abrupt enhancement during later months may indicate a shift in ISM season due to a warmer climate. The PDF distribution of different category rainfall events found RegCM4.7 performing satisfactorily over IGP during the historical period. Most distribution is shifting towards the higher rainfall amount in NF and FF. Similarly, all the experiments satisfactorily simulated the distribution patterns of rainfall extremes. However, the RegCM with EIN75 and MPI-ESM-MR shows more realistic results in simulating all category rainfall events (especially RHR and HR events), and the performance of RegCM_MIROC improved as we move towards VHR and EHR events. The RegCM under the warming scenario projects a moderate to a higher but significant decrease in RHR events. In contrast, several HR, VHR, and EHR categories have moderate to higher significant enhancement over IGP regions. At the same time, the relative changes in mean thresholds of the most devastating rainfall category, i.e., EHR, are expected to get enhanced during NF and FF. This suggests that the extreme rainfall events over IGP are rising and intensifying under intense warming climatic conditions. It is found that the changes in several events during FF

are less prominent than NF, possibly due to the previously defined fact that monsoon regimes may shift towards later months of the year. A comprehensive analysis of various thermodynamical and dynamical quantities has been performed to support and understand the mechanism behind rainfall extremes in present and future time scales. The RegCM4.7 satisfactorily represents the evolution mechanism of monsoon extremes over the IGP region. An abrupt TG and atmospheric moisture content enhancement during the extreme event days in NF and FF has been projected under the high-emission RCP8.5 scenario. However, the weakening of ISM circulation and LPS in NF and FF as compared with the historical period have been projected. This study explores the observed and modeling aspects of ISMR and associated extremes over the IGP region during the past and future under high-emission scenarios. The detailed spatiotemporal patterns of past and future climate extremes are assessed and analyzed in this study to strengthen the decision-making capability of government and policymakers to adapt and better prepare for the effects on the near and far future, particularly in the water and agricultural sectors for a socioeconomically vulnerable region (here IGP) and hence the country.

Author contributions The idea of the present study is proposed by MP and SG, and is designed by SG, MP, and RB. SD provided the model-simulated data sets, and MP did the data processing. MP, SG, SD, and RB analyzed the data and visualized it by MP and SG. MP wrote the first draft, which SG subsequently modified. The work is investigated by MP, SG, and SD, and supervised by RB and RKM. All the authors have read the manuscript, provided their expertise to improve the work quality, and accepted the author's agreement. There is no conflict of interest.

Availability of data and material The datasets generated and the codes used during the analysis for the study are available from the corresponding author upon reasonable request.

Declarations

Conflict of interest The authors declare that they have no competing interests.

Ethics approval and consent to participate Not applicable.

Consent for publication Not applicable.

References

Adel MM (2002) Man-made climatic changes in the Ganges basin. Int J Climatol J R Meteorol Soc 22(8):993–1016

Ajayamohan R, Rao SA (2008) Indian ocean dipole modulates the number of extreme rainfall events over India in a warming environment. J Meteorol Soc Jpn Ser II 86(1):245–252

Ali H, Mishra V, Pai D (2014) Observed and projected urban extreme rainfall events in India. J Geophys Res Atmos 119(22):12–621

Amin M, Rizwan M, Alazba A (2016) A best-fit probability distribution for the estimation of rainfall in northern regions of Pakistan. Open Life Sci 11(1):432–440

Annamalai H, Sperber K (2005) Regional heat sources and the active and break phases of boreal summer intraseasonal (30–50 day) variability. J Atmos Sci 62(8):2726–2748

Ashfaq M, Cavazos T, Reboita MS et al (2021) Robust late twenty-first century shift in the regional monsoons in regcm-cordex simulations. Clim Dyn 57:1463–1488

Barde V, Nageswararao M, Mohanty U et al (2020) Characteristics of southwest summer monsoon rainfall events over east India. Theoret Appl Climatol 141:1511–1528

Bentsen M, Bethke I, Debernard JB et al (2013) The Norwegian earth system model, noresm1-m-part 1: description and basic evaluation of the physical climate. Geosci Model Dev 6(3):687–720

Bhatla R, Ghosh S, Mandal B et al (2016) Simulation of Indian summer monsoon onset with different parameterization convection schemes of regcm-4.3. Atmos Res 176:10–18

Bhatla R, Ghosh S, Mall R et al (2018) Regional climate model performance in simulating intra-seasonal and interannual variability of Indian summer monsoon. Pure Appl Geophys 175:3697–3718

Bhatla R, Ghosh S, Verma S et al (2019) Variability of monsoon over homogeneous regions of India using regional climate model and impact on crop production. Agric Res 8:331–346

Bollasina MA, Ming Y, Ramaswamy V (2011) Anthropogenic aerosols and the weakening of the south Asian summer monsoon. Science 334(6055):502–505

Boyaj A, Ashok K, Ghosh S et al (2018) The Chennai extreme rainfall event in 2015: the bay of Bengal connection. Clim Dyn 50:2867–2879

Collins M, Knutti R, Arblaster J et al (2013) Long-term climate change: projections, commitments and irreversibility. Cambridge University Press, Cambridge

Das S, Giorgi F, Giuliani G (2020) Investigating the relative responses of regional monsoon dynamics to snow darkening and direct radiative effects of dust and carbonaceous aerosols over the indian subcontinent. Clim Dyn 55:1011–1030

Dash S, Pattnayak K, Panda S et al (2015) Impact of domain size on the simulation of Indian summer monsoon in regcm4 using mixed convection scheme and driven by hadgem2: impact of domain size on ism simulations. Clim Dyn 44:961–975

Dash S, Kulkarni MA, Mohanty U et al (2009) Changes in the characteristics of rain events in India. J Geophys Res Atmos 114(D10)

Elguindi N, Bi X, Giorgi F et al (2013) Regional climate model regcm user manual version 4.4. The Abdus Salam International Centre for Theoretical Physics, Strada Costiera, Trieste, Italy October 21(2013), p 54

Emanuel KA, Živković-Rothman M (1999) Development and evaluation of a convection scheme for use in climate models. J Atmos Sci 56(11):1766–1782

Fadem B (2012) High-yield behavioral science. Lippincott Williams & Wilkins, Pennsylvania

Field CB, Barros V, Stocker TF et al (2012) Managing the risks of extreme events and disasters to advance climate change adaptation: special report of the intergovernmental panel on climate change. Cambridge University Press, Cambridge

Gadgil S (2003) The Indian monsoon and its variability. Annu Rev Earth Planet Sci 31(1):429–467

Ghosh S, Das D, Kao SC et al (2012) Lack of uniform trends but increasing spatial variability in observed Indian rainfall extremes. Nat Clim Chang 2(2):86–91

Ghosh S, Bhatla R, Mall R et al (2019) Aspect of ecmwf downscaled regional climate modeling in simulating Indian summer monsoon rainfall and dependencies on lateral boundary conditions. Theoret Appl Climatol 135:1559–1581

Ghosh S, Sinha P, Bhatla R et al (2022) Assessment of lead-lag and spatial changes in simulating different epochs of the Indian summer monsoon using regcm4. Atmos Res 265(105):892

Ghosh S, Miller AJ, Subramaniam AC et al (2023) Signals of northward propagating monsoon intraseasonal oscillations (misos) in the regcm4. 7 cordex-core simulation over south Asia domain. Clim Dyn:1–15

Giorgi F, Coppola E, Solmon F et al (2012) Regcm4: model description and preliminary tests over multiple cordex domains. Clim Res 52:7–29

Goswami BN, Venugopal V, Sengupta D et al (2006) Increasing trend of extreme rain events over India in a warming environment. Science 314(5804):1442–1445

Grenier H, Bretherton CS (2001) A moist pbl parameterization for large-scale models and its application to subtropical cloud-topped marine boundary layers. Mon Weather Rev 129(3):357–377

Joseph S, Sahai A, Sharmila S et al (2015) North Indian heavy rainfall event during June 2013: diagnostics and extended range prediction. Clim Dyn 44:2049–2065

Kiehl J, Hack J, Bonan G et al (1996) Description of the ncar community climate model (ccm3). technical note. Tech. rep., National Center for Atmospheric Research, Boulder, CO (United States)

Koshal AK (2014) Changing current scenario of rice-wheat system in Indo-Gangetic plain region of India. Int J Sci Res Publ 4(3):1–13

Kothyari U, Singh V, Aravamuthan V (1997) An investigation of changes in rainfall and temperature regimes of the ganga basin in India. Water Resour Manage 11:17–34

Krishnan R, Sanjay J, Gnanaseelan C et al (2020) Assessment of climate change over the Indian region: a report of the ministry of earth sciences (MOES), government of India. Springer Nature, Berlin

Kulkarni A (2012) Weakening of Indian summer monsoon rainfall in warming environment. Theoret Appl Climatol 109:447–459

Kumar KK, Rajagopalan B, Hoerling M et al (2006) Unraveling the mystery of Indian monsoon failure during el niño. Science 314(5796):115–119

Kumar A, Dudhia J, Rotunno R et al (2008) Analysis of the 26 July 2005 heavy rain event over Mumbai, India using the weather research and forecasting (wrf) model. Q J R Meteorol Soc 134(636):1897–1910

Lal P, Shekhar A, Gharun M et al (2023) Spatiotemporal evolution of global long-term patterns of soil moisture. Sci Total Environ:161470

Lau WKM, Waliser DE (2011) Intraseasonal variability in the atmosphere-ocean climate system. Springer, Berlin

Maharana P, Dimri A, Choudhary A (2020) Future changes in Indian summer monsoon characteristics under 1.5 and 2 c specific warming levels. Clim Dyn 54:507–523

Mishra V, Shah HL (2018) Hydroclimatological perspective of the Kerala flood of 2018. J Geol Soc India 92:645–650

Mishra V, Aadhar S, Asoka A et al (2016) On the frequency of the 2015 monsoon season drought in the Indo-Gangetic plain. Geophys Res Lett 43(23):12–102

Mishra AK, Dwivedi S, Das S (2020) Role of Arabian sea warming on the Indian summer monsoon rainfall in a regional climate model. Int J Climatol 40(4):2226–2238

Mukherjee S, Aadhar S, Stone D et al (2018) Increase in extreme precipitation events under anthropogenic warming in India. Weather Clim Extremes 20:45–53

Ngo-Duc T, Tangang FT, Santisirisomboon J et al (2017) Performance evaluation of regcm4 in simulating extreme rainfall and temperature indices over the cordex-southeast asia region. Int J Climatol 37(3):1634–1647

Nikumbh AC, Chakraborty A, Bhat G (2019) Recent spatial aggregation tendency of rainfall extremes over india. Sci Rep 9(1):10321

Oleson K, Lawrence D, Bonan G et al (2013) Technical description of version 4.5 of the community land model (clm)(ncar technical note no. ncar/tn-503+ str). citeseer. National Center for Atmospheric Research, PO Box 3000:555

Pai D, Rajeevan M, Sreejith O et al (2014) Development of a new high spatial resolution (0.25 × 0.25) long period (1901–2010) daily gridded rainfall data set over India and its comparison with existing data sets over the region. Mausam 65(1):1–18

Pal JS, Small EE, Eltahir EA (2000) Simulation of regional-scale water and energy budgets: representation of subgrid cloud and precipitation processes within regcm. J Geophys Res Atmos 105(D24):29579–29594

Pant M, Ghosh S, Verma S et al (2022) Simulation of an extreme rainfall event over Mumbai using a regional climate model: a case study. Meteorol Atmos Phys 134:1–17

Pant M, Bhatla R, Ghosh S et al (2023) Will warming climate affect the characteristics of summer monsoon rainfall and associated extremes over the Gangetic plains in India? Earth Sp Sci 10(2):e2022EA002741

Parth Sarthi P, Ghosh S, Kumar P (2015) Possible future projection of Indian summer monsoon rainfall (ismr) with the evaluation of model performance in coupled model inter-comparison project phase 5 (cmip5). Global Planet Change 129:92–106

Parth Sarthi P, Kumar P, Ghosh S (2016) Possible future rainfall over Gangetic plains (gp), India, in multi-model simulations of cmip3 and cmip5. Theoret Appl Climatol 124:691–701

Pattanaik D, Rajeevan M (2010) Variability of extreme rainfall events over India during southwest monsoon season. Meteorol Appl J Forecast Pract Appl Train Tech Model 17(1):88–104

Piao S, Yin L, Wang X et al (2009) Summer soil moisture regulated by precipitation frequency in china. Environ Res Lett 4(4):044012

Rai P, Singh G, Dash S (2020) Projected changes in extreme precipitation events over various subdivisions of India using regcm4. Clim Dyn 54:247–272

Rajeevan M, Bhate J, Jaswal AK (2008) Analysis of variability and trends of extreme rainfall events over India using 104 years of gridded daily rainfall data. Geophys Res Lett 35(18)

Rajeevan M, Gadgil S, Bhate J (2010) Active and break spells of the Indian summer monsoon. J Earth Syst Sci 119:229–247

Reshma T, Varikoden H, Babu C (2021) Observed changes in Indian summer monsoon rainfall at different intensity bins during the past 118 years over five homogeneous regions. Pure Appl Geophys 178:3655–3672

Roxy MK, Ritika K, Terray P et al (2014) The curious case of Indian ocean warming. J Clim 27(22):8501–8509

Roxy MK, Ritika K, Terray P et al (2015) Drying of Indian subcontinent by rapid Indian ocean warming and a weakening land-sea thermal gradient. Nat Commun 6(1):7423

Roxy MK, Ghosh S, Pathak A et al (2017) A threefold rise in widespread extreme rain events over central India. Nat Commun 8(1):1–11

Shahi NK, Das S, Ghosh S et al (2021) Projected changes in the mean and intra-seasonal variability of the Indian summer monsoon in the regcm cordex-core simulations under higher warming conditions. Clim Dyn 57:1489–1506

Sharmila S, Joseph S, Sahai A et al (2015) Future projection of Indian summer monsoon variability under climate change scenario: an

assessment from cmip5 climate models. Global Planet Change 124:62–78

Singh N, Sontakke N (2002) On climatic fluctuations and environmental changes of the Indo-Gangetic plains, India. Clim Change 52:287–313

Singh D, Tsiang M, Rajaratnam B et al (2014) Observed changes in extreme wet and dry spells during the south Asian summer monsoon season. Nat Clim Chang 4(6):456–461

Sinha R, Jain V (1998) Flood hazards of north Bihar rivers, Indo-Gangetic plains. Mem Geol Soc India:7–52

Sinha P, Mohanty U, Kar S et al (2013) Sensitivity of the gcm driven summer monsoon simulations to cumulus parameterization schemes in nested regcm3. Theoret Appl Climatol 112:285–306

Sinha P, Maurya R, Mohanty M et al (2019) Inter-comparison and evaluation of mixed-convection schemes in regcm4 for Indian summer monsoon simulation. Atmos Res 215:239–252

Stevens B, Giorgetta M, Esch M et al (2013) Atmospheric component of the mpi-m earth system model: Echam6. J Adv Model Earth Syst 5(2):146–172

Stocker T (2014) Climate change 2013: the physical science basis: working group I contribution to the fifth assessment report of the intergovernmental panel on climate change. Cambridge university press

Tabari H (2020) Climate change impact on flood and extreme precipitation increases with water availability. Sci Rep 10(1):1–10

Taylor KE, Stouffer RJ, Meehl GA (2012) An overview of cmip5 and the experiment design. Bull Am Meteor Soc 93(4):485–498

Tiedtke M (1989) A comprehensive mass flux scheme for cumulus parameterization in large-scale models. Mon Weather Rev 117(8):1779–1800

Trenberth KE, Dai A, Rasmussen RM et al (2003) The changing character of precipitation. Bull Am Meteor Soc 84(9):1205–1218

Verma S, Bhatla R (2021) Performance of regcm4 for dynamically downscaling of el nino/la nina events during southwest monsoon over India and its regions. Earth Sp Sci 8(3):e2020EA001474

Verma S, Bhatla R, Ghosh S et al (2021) Spatio-temporal variability of summer monsoon surface air temperature over India and its regions using regional climate model. Int J Climatol 41(13):5820–5842

Watanabe S, Opper M (2010) Asymptotic equivalence of bayes cross validation and widely applicable information criterion in singular learning theory. J Mach Learn Res 11(12)

Wei J, Su H, Yang ZL (2016) Impact of moisture flux convergence and soil moisture on precipitation: a case study for the southern united states with implications for the globe. Clim Dyn 46:467–481

Willmott CJ (1981) On the validation of models. Phys Geogr 2(2):184–194